EUROPEAN ORGANIZATION FOR NUCLEAR RESEARCH

CERN DRDC/94-4
DRDC/P-54
5 January 1994

R&D Proposal
Development of Quartz Fiber Calorimetry

A. Contin*,a), G. Lacommare, M. Marino, R. DeSalvo**), A. Zichichi
CERN/LAA, Geneva, Switzerland

D. Brozzi, J.P. Poitier, L. Rinolfi, J.C. Santiard, M. Tavlet
CERN, Geneva, Switzerland

M. Lundin, M.R. Mondardini
Cornell University, Ithaca, NY, USA

J. Britz, R. Glassmann, P. Gorodetzky*,b), J.M. Helleboid, M.F. Janot, P. Juillot, P. Schuller, B. Speckel
CRN Strasbourg, France

F. Arzarello, G. Bari, M. Basile, L. Bellagamba, D. Boscherini, G. Bruni, P. Bruni, G. Cara Romeo, M. Chiarini, F. Cindolo, F. Ciralli, P. Giusti, G. Iacobucci, G. Laurenti, G. Maccarrone, A. Margotti, T. Massam, R. Nania, G. Sartorelli, R. Timellini
INFN Bologna and University of Bologna, Italy

G. Anzivino, S. De Pasquale
INFN Laboratori Nazionali di Frascati, Italy

M. Rossella[c)]
INFN Pavia, Italy

L. Cifarelli,
University of Pisa and INFN Bologna, Italy

M. Dardo, G. Dellacasa, M. Gallio, A. Musso
University of Torino and INFN Torino, Italy

K.F. Johnson, D. Lazic
Florida State University, Tallahassee, FL, USA

S. Bojarinov, Yu. Chumarovsky[e], M. Danilov, V. Gavrilov, A. Golutvin, V. Isaev[e], V. Izraelyan[e], S. Kuleshov, D. Litvintsev, S. Morshnev[e], V. Rusinov, O. Ryabushkin[e], A. Smirnitsky, V. Stolin, M. Vinogradov, Yu. Zemskov[e]
ITEP, Moscow, Russia [d]

C. Fuchs, Z. Kuznicki, J.P. Ponpon, P. Siffert
PHASE, Strasbourg, France

Abstract

Very Forward Calorimeters (VFCs) in LHC detectors should cover the pseudorapidity range from $\eta = 2.5$ to at least $\eta = 5$ in order to compute missing transverse energy and for jet tagging. Operation at such high rapidity requires the use of a calorimetry technique that is very radiation resistant, fast and insensitive to radioactivity (especially to neutrons). This can be accomplished through the Quartz-Calorimeter (Q-Cal) concept of embedding silica core fibers, that resist to the Gigarad radiation level, into an absorber. In this calorimeter the shower particles produce light through the Cherenkov effect generating a signal less than 10 ns in duration. Unique to this new technology, the visible energy of hadronic showers has a transverse dimension nearly an order of magnitude smaller than that in conventional calorimeters, enabling precise spatial resolution, sharper isolation cuts and better jet recognition against the minimum bias events background. Last but not least, most radioactive decays and neutron interactions produce particles below the Cherenkov threshold; therefore, this calorimeter is intrinsically insensitive to radio-activation background.
All of these characteristics taken together allow the Q-Cal to be operated meaningfully in the extreme working conditions of a VFC at LHC.
The purpose of this R&D proposal is an in depth study of the performances of different kinds of silica fibers in the presence of radiation load, a study of customized ultra-violet (UV) photodetectors (and especially pixelised Hybrid Photo Diodes (HPD)) and construction and beam testing of suitable calorimeter prototypes: a few small electromagnetic prototypes, and finally a hadronic prototype with all the features required for a VFC (with the exception of the transverse size): radiation resistance, speed, spatial resolution, transverse energy (E_T) measurement and implementation of an E_T trigger.
The end product of the proposed research program will be a proof of feasibility and the collection of basic information necessary for the design of a Very Forward Calorimeter at LHC.

---

*) Spokespersons.
**) Contact person.
[a] also University of Bologna, Italy.
[b] at CERN from March 1994.
[c] presently at CRN, Strasbourg, France.
[d] also supported by the State Program on Fundamental Nuclear Physics.
[e] actually at IRE, Moscow.

Contents

1 INTRODUCTION.

Detectors for a future hadron supercollider must satisfy demanding requirements in order to face the challenge of performing meaningful experiments in a severe environment. Calorimeters will be the heart of new experiments and will play a fundamental role in measuring and localizing the energy flow of events, identifying leptons, measuring missing energy. In addition, calorimeters will provide the main trigger. Therefore, they should have a good energy resolution, a fast, linear and uniform response, and be hermetic and radiation resistant.

The nearly flat azimuthal angle and rapidity production distributions of particles in hadron-hadron interactions imply that the calorimeter system should extend towards very small angles with respect to the outgoing beam directions, still satisfying as much as possible the requirements listed above. The physics goals of the experiments, the intrinsic physics limitations, the interaction rate and the availability of space may somehow relax these requirements.

In section 2, some of the physics goals of a multi-TeV hadron Collider are briefly reviewed with particular emphasis on the forward direction. In section 3 the main characteristics of the quartz fiber calorimeter (Q-Cal in the following) are presented and compared to the goals defined in section 2. Sections 4 reviews the present knowledge on quartz fiber calorimetry. Section 5 describes a possible design for a Very Forward Calorimeter (VFC in the following) at LHC, covering the region $2.5 < | \eta | < 5$. Section 6 and 7 summarize the R&D needed to fully develop this technique and the proposed R&D program. Finally, section 8 presents the division of responsibilities between the collaboration and the requested budget.

The R&D program proposed here (extending over two years), is independent of a specific detector. Only in a second phase, when enough knowledge is gathered, will the solutions be adapted to specific detectors.

Keen interest on this technology has already been shown by the presently proposed LHC detectors (ATLAS, CMS and ALICE) and by the heavy ion experiments at RHIC (BRAHMS, PHENIX and STAR). The authors would like to thank some of the spokesmen of the LHC LOIs for their positive evaluation of our ideas and their encouragement to develop them, to present, which helped to obtain the scientific approval from national funding agencies.

2 PHYSICS GOALS AND ENVIRONMENTAL CONSTRAINTS.

Broadly speaking, the physics goals of future experiments in multi-TeV hadron colliders are threefold:

a) to study particle and jet production up to the highest possible energy,
b) to solve the problem of the electroweak symmetry breaking mechanism, via the production and the detection of Higgs boson(s),
c) to explore possible extensions of the Standard Model, e.g. supersymmetry (SUSY),
d) measurement of top production.

As the point-like cross-section between hadron constituents falls very rapidly with increasing energy, the processes b) and c) are affected by a large background due to softer col-

lisions. Dedicated, low-luminosity measurements are of paramount importance to determine the background shape and to disentangle, with the help of complete MonteCarlo simulations, the interesting signals from the almost overwhelming background.

Due to practical limitations on the bunch spacing of the collider, multiple interactions per bunch crossing are expected when running at the highest luminosities. Several "minimum bias" events will overlap with one interesting event produced in the same bunch crossing, hence diluting physics signatures.

The detector and, in particular, the forward part of the calorimeter system (VFC), must be able to operate in two different regimes:

- high cross-section/low luminosity with one or less events per bunch crossing,
- low cross-section/high-luminosity with several events per bunch crossing.

The former case corresponds mainly to background and top-quark production studies, the latter to more attractive and rare physics for which the first example is regarded as a background. Each regime calls for specific forward calorimeter characteristics which will be briefly illustrated in the following sections.

2.1 Low luminosity physics.

The production distribution of particles in proton-proton interactions is nearly flat in rapidity (or pseudorapidity). The width of the rapidity "plateau" depends on the total centre-of-mass energy, and extends to about ± 6 units (at half maximum) at LHC.

In an ideal detector the performance of the calorimeter should remain the same over all the rapidity coverage (e.g. for $\mid \eta \mid < 5$). In particular, to have consistent jet reconstruction and lepton isolation capabilities, the sizes of hadronic and electromagnetic showers, measured as $\Delta\eta$, should be nearly constant even in the forward direction highly compressed phase space. This can be partially achieved by moving the VFC ($2.5 < \mid \eta \mid < 5$) further away from the interaction region. Figure 1a shows the hadronic shower size, in $\Delta\eta$, for a dense dE/dx-based calorimeter (e.g. lead/scintillating fibers with a density of $8 \div 9$ g/cm^3, with lateral, hadronic shower size of ~ 25 cm at 95% collection efficiency) as a function of η, for the very simple geometry sketched in Fig. 1b. The relative size of the shower increases rapidly above $\eta = 3$ thus deteriorating the detector performances. Therefore, the first conclusion is that the (visible) showers in the VFC should be at least a factor ten narrower than in a standard calorimeter.

We anticipate here one of the main advantages of the Q-Cal. As only superluminal particles (i.e. those with velocity above the Cherenkov threshold) produce light, and because of the limited angular acceptance of the fibers, the visible size of hadronic showers is only $3 \div 4$ cm (at 95% collection efficiency - see section 4.2). The dash-dotted line in Fig. 1a shows the shower size in $\Delta\eta$ if a Q-Cal is used as VFC.

When increasing the hardness of the fundamental parton-parton interaction, QCD jet production becomes dominant. QCD jets are abundantly produced: several events per day are expected at a luminosity of $10^{33}\,\mathrm{cm}^{-2}\,\mathrm{s}^{-1}$ in the rapidity range $3 < \mid \eta \mid < 5$ and with transverse momentum (p_T) greater than $500\,GeV$ [1]. A complete measurement of these jets will give precious information on the background expected in rarer channels.

The characteristics of high p_T jets emitted in the forward direction have been studied

using the PYTHIA5.6/JETSET7.3 MonteCarlo simulation package [2]. Interactions were selected with at least one primary parton emitted with $3 < |\eta| < 4$ and $200 < p_T < 300$ GeV. Jets were then reconstructed using the standard JETSET7.3 routines with the following parameters:

- calorimeter cells granularity: $\Delta\eta \times \Delta\phi = 0.05 \times 0.05$,
- seed cell minimum energy: 1.5 GeV,
- cone aperture: $\Delta R = \sqrt{\Delta\eta^2 + \Delta\phi^2} < 0.7$,
- minimum jet energy: 10 GeV.

These "jets", whose energy peaks at about 2.5 TeV, were then compared with the primary partons originating them. Figures 2a and b show the energy flow (normalized to the primary parton energy) and the integrated normalized energy as a function of the distance from the reconstructed jet axis, respectively. About 96% of the primary parton energy is collected in a cone aperture $\Delta R = \sqrt{\Delta\eta^2 + \Delta\phi^2} < 0.7$. The relative difference between the reconstructed and the primary energy is shown in Fig. 3. Fluctuation due to the jet reconstruction algorithm limits the energy resolution for jets to about 6% (r.m.s) at TeV energies.

The flux of particles as a function of the radial distance from the jet axis is shown in Fig. 4. More than one particle/cm is expected in the jet core.

As for the measurement of top production, the cross section is so high ($\sigma(pp \to tt) \sim 5 \times 10^3$ pb) that most of the studies can be performed at low luminosity ($< 10^{33}\,\mathrm{cm}^{-2}\,\mathrm{s}^{-1}$). Detection strategies include the study of the decays:

$$tt \to WbWb \to \ell\nu bb\,\mathrm{jet\,jet}$$
$$tt \to WbWb \to \ell\nu\ell\nu bb.$$

Although, in general, backgrounds to these channels extend to higher rapidities than the signal, a VFC with the same performances in terms of lepton and jet detection and lepton isolation capabilities as the central detector will help in increasing the statistics of detected top decays and in studying the production mechanism of top quarks in a wider phase space region (making the reduction of shower dimensions of fundamental importance). In this respect it is worth noting that about 25% of the decays $tt \to WbWb \to \ell\nu\ell\nu$ jet jet (PYTHIA5.6 simulation program, $m_t = 150$ GeV) produce at least one lepton with $|\eta| > 2.5$, and that this fraction increase to 50% if at least one top quark is required to be produced with $|\eta| > 2.5$. More simulations are required to completely assess the effect of VFC on top studies.

2.2 High luminosity physics.

The two main justifications for a VFC in the high-luminosity operation of a multi-TeV hadron collider are:

- to improve hermiticity for missing transverse energy measurements,
- to tag forward jets for event selection.

A non-zero, vectorial sum of all transverse momenta of the particles produced in the interaction is an important signature for the presence of non-interacting particles like neutrinos and the lightest supersymmetric particle. The possibility to detect such particles depends

on the process, on the rapidity coverage, energy and position resolution of the calorimeter and on the background level.

A benchmark process is the high-mass Higgs boson decay $H \rightarrow ZZ \rightarrow \ell\ell\nu\nu$, in which the two neutrinos appear as missing energy of the event. MonteCarlo simulations [3] show that, in order to reduce the background level below the signal, a rapidity coverage down to $\eta = 4$ is mandatory (see Fig. 5). The effect of the calorimeter energy resolution on missing energy event selection is very low [4]: as the rapidity changes quickly with position, the calorimeter positioning capability is more important than energy resolution. Small shower dimensions are important not to let the signal smear over a too wide a rapidity span and also in applying isolation cuts.

The possibility of tagging forward jets down to 5 in rapidity opens up the possibility to study the production of high-mass ($m_H > 500$ GeV) Higgs bosons from WW or ZZ fusion. In these events, the outgoing jets have radiated a W boson, i.e. their transverse momentum is on the order of m_W, but have large longitudinal momentum (> 1 TeV). Therefore, their rapidity distribution peaks in the range $| \eta | = 2 \div 5$ (see Fig. 6). When looking at the Higgs decay $H \rightarrow WW \rightarrow \ell\nu + 2jets$, the requirement of the presence of two jets with $| \eta | > 3.5$ reduces significantly the QCD background [5].

The main problem facing calorimetry at high rapidity in very high luminosity operations is the pile-up from the minimum bias events which overlap the interesting event in each crossing. For example, with the design LHC luminosity of $1.7 \times 10^{34}\,\mathrm{cm}^{-2}\,\mathrm{s}^{-1}$, about 40 minimum bias (including diffractive) events will be produced per bunch crossing. Their energy flow is shown in Fig. 7 as a function of η. The fluctuations on this energy cause a degradation in the energy resolution of the calorimeter due to pile-up in single cells. Figure 8 shows the added resolution due to pile-up as a function of the jet p_T in the η range $2.5 \div 5$ and for two values of luminosity, $1.7 \times 10^{34}\,\mathrm{cm}^{-2}\,\mathrm{s}^{-1}$ (40 minimum bias events per crossing) and $0.6 \times 10^{34}\,\mathrm{cm}^{-2}\,\mathrm{s}^{-1}$ (15 minimum bias events per crossing).

Here also, the conclusion is that a modest calorimeter resolution (constant term $\sim 5 \div 10\%$) can be adequate to the physics needs.

2.3 Environmental constraints.

Other, very tight, constraints come as a consequence of the high luminosity operation and of the bunch structure of multi-TeV hadron colliders.

2.3.1 Radiation hardness.

At the nominal LHC luminosity ($1.7 \times 10^{34}\,\mathrm{cm}^{-2}\,\mathrm{s}^{-1}$), the VFCs, covering a pseudorapidity range from 2.5 to 5 will be exposed to doses reaching 160 Mrad per year (10^7 s) of operation. The maximum dose is reached in the first 20 cm from the calorimeter front face and at a pseudorapidity of 4.5 to 5, mostly due to the electromagnetic energy deposited by the minimum bias events present in each crossing [6]. It is therefore mandatory that the VFCs keep their properties to at least 1 Grad integrated over 5 years of operation.

2.3.2 Insensitivity to low energy neutrons.

The neutrons produced in the hadronic showers also create a very severe background [7] in standard calorimetry. Fluxes reach a few $10^{15}\,\mathrm{n/cm^2/year}$, the neutron energies range

roughly from 1 eV to some MeV. The neutrons arrive in the active elements of the VFC after a delay [8, 17] of up to 1000 ns and can induce, in standard dE/dx-based calorimeters, an asynchronous signal whose amplitude may locally be greater than that of the minimum bias induced showers. It could be noted as an example, that, in the case of ATLAS, the collimators protecting the low beta quadrupoles are inside the VFCs and increase the neutron fluxes to the point that no electronics should be placed behind these calorimeters. Conclusion: VFCs should be insensitive to neutrons.

2.3.3 Insensitivity to radio-activation.

A lesser but still formidable problem is presented by the signal generated by radio-activation of the absorber material. The VFC should be made with the least activatable materials and be insensitive to radioactive decays.

2.3.4 Safety.

There is no doubt that the VFC will receive a very high dose and will become quite radioactive. For safety reasons, it should not contain liquids or gases that might become radioactive and all radio-activated products should remain contained in the calorimeter itself.

2.3.5 Speed.

The time interval between crossings is 25 ns. The occupancy, especially at high rapidities, is very large due to the minimum bias events present at each crossing. An interesting event should not suffer from pile-up generated by previous crossings. Therefore, all the VFC signals at the digitizer input should be back to zero in less than 20 ns without ringing.

2.4 Zero degree measurement for heavy ion collisions.

LHC will accelerate heavy ions up to lead: ALICE [9] has been proposed as a dedicated heavy ion experiment, but the other proposed experiments will also use these beams which could shed light on the exotic phase of nuclear matter called quark-gluon plasma. The luminosity would be much lower than for p-p collisions, so that the problems are not the same. In order to know the energy actually deposited in the collision, the energy of the spectator nuclei should be measured. It is impossible to detect the fragments with Z/A on the same order as for the beams because they remain in the beam pipe (and this is valid probably for $Z/A = 0.5$), but, fortunately, a good image of all the spectators is given by the spectator neutrons. These neutrons can be detected at zero degrees with two hadron calorimeters placed on each side of the LHC detector, between the two final dipoles. As the transverse space is very small, such a detection and measurement are possible only if the hadronic transverse shower size seen by this zero degree calorimeter is very small, to a point where the visible lateral shower leakage is negligible. With the actual design of the dipoles, the observed showers should be contained in less than 10 cm. It will be shown later that this is an easy goal for the Q-Cal technique, while it is almost impossible for any other technique.

Another interesting phenomenon to be measured in heavy ions colliders is the soft photon production due to the bremsstrahlung of the struck nucleons in a heavy ion collision [9, 10]. These photons are emitted in a cone of 1 mrad opening meaning they would also strike the zero degree calorimeter. Their total energy amounts to 20 TeV for a central lead-lead

collision. A fine z-granularity, for the best electron-hadron separation, is the main ingredient for this measurement yielding in a redundant way the energy deposited in the collision.

The same problems outlined in this chapter are relevant also to the BNL heavy ion collider RHIC [11].

3 THE Q-CAL SOLUTION.

The Q-Cal Collaboration was started in 1993 by several members of the present proposal. Its goal is to promote quartz[1)] fiber calorimetry. A few papers were written and two doctoral thesis have already been generated on this subject [12, 13, 14, 15, 16, 17, 18, 19] inside Q-Cal.

3.1 Radiation hardness.

Historically, our interest in quartz fiber calorimetry initiated because of the radiation hardness of quartz. Figure 9 shows the transparency of a 3 mm thick Suprasil-2 silica disc versus irradiation dose measured at GANIL with a 100 MeV/n oxygen beam [13]. It can be seen that an annealing appears after a few hundred Mrad. Furthermore, most of the damage is outside the wavelength range of the UV sensitive photomultiplier tube (PMT) Philips 2020/Q. The experiment NA38 at CERN (quark-gluon plasma search through dimuon measurement) uses the same "quartz" to tag and center the sulfur beam just before the targets. Up to now, the integrated radiation dose is more than 12 Grad and the voltage of the PMTs has not been changed since the beginning. So, this material is radiation hard and silica core fibers should also be radiation hard.

3.2 The Cherenkov effect in fibers – Simulation program.

Figure 10 shows schematically the Cherenkov effect in an optical fiber. A simulation of the number of produced photons is shown in Fig. 11 as a function of α, the angle between the particle trajectory and the fiber and b, the "impact parameter" or distance between the fiber center and the particle trajectory. In Fig. 11, the fiber's numerical aperture is 0.37 and the particle velocity is $\beta = 1$. The multiple scattering of the particle in the fiber has been neglected, which, for our uses, was shown to be a good approximation. In this calculation it is taken into account that the spiraling photons, created by a particle with α close to 0° and large impact parameter, do not exit the fiber but are reflected back at its extremity by total internal reflection (i.e. these photons are never detected). If the shower core must be detected, the best working angle is around 45°. Figure 12 shows the same yield as a function of α and β (integrated over all impact parameters, b). It can be seen that, except close to the Cherenkov threshold, the optimal angle does not vary much. The peak at $\alpha = 0°$ (parallel to the fibers) is fictitious for it corresponds to particles at the threshold, i.e. 150 keV electrons, travelling a long way into the fiber, while in reality they have a very small mean free path in the silica.

A GEANT simulation program has been developed with a careful study of the hadronic and electromagnetic cuts. The shower particles are tracked in the absorber until they touch

[1)] The denomination "quartz" is actually improper for it refers to a crystal. Technically, the correct term is "amorphous silica," usually referred to as silica. Here we use the terms quartz and silica to refer to amorphous silica.

a fiber. Multiple scattering and interactions are neglected in the fiber for CPU time reasons. The α, β and b particle-fiber parameters are then used to obtain the resulting number of photons from the same tables used to produce Figs. 11 and 12. The exit point of the particle in the fiber is then computed and returned to GEANT. The tables also give the transport velocity of light inside the fibers. Figure 13 shows the result of this Monte-Carlo for the NA50 zero degree calorimeter application where the calorimeter is segmented every 28 cm in z. When the anode signals are delayed by the same time that the shower propagates (1 ns/28 cm), the resulting total pulse is back to zero in less than 5 ns. Another good feature is the excellent linearity shown in Fig. 14. It is a consequence of a good shower containment and the fact that Cherenkov effect does not exhibit saturation.

4 WHAT IS KNOWN.

4.1 Radiation hardness.

Figure 15 shows the light yield of 3 types of silica fibers[2)] irradiated by 2 MeV electrons up to 2.3 Grad. The light was produced by the Cherenkov effect of the electrons passing through the fibers at 45°. The r.m.s. width of the beam was $\sim$ 3 cm. The whole fiber, which was 1.0 m long, suffered a more or less constant irradiation of 1/10 of the maximum irradiation. This exposure pattern mimics well the predicted irradiation in a VFC. The light was directed on a paper screen and then detected by a high quality CCD camera with classical, visible light optics. No loss can be seen for the silica clad fibers, while the doped PMMA clad fibers lose transmission after 700 Mrad due to plastic reticulation. No change in numerical aperture could be observed within the resolution of this experiment (10%). Also ref. [20] shows what is known in general when a long (more than 10 m) fiber is irradiated (with a ^{60}Co source) constantly along its total length. In addition, at ITEP, some fibers were irradiated and tested with a N_2 (UV) laser and results are forthcoming.

A pilot radiation damage test was started at LIL in December 1993. The purpose of this test is to get a glimpse of quartz fiber radiation hardness in real working conditions, and to develop a testing protocol for the future. In the test, the loss of transparency over a $7 \div 10$ cm long exposed section is measured with a photodetector (sensitive in the same wavelength region as photodetectors foreseen for use in a real experiment). Both Cherenkov signal and radiation damage are generated by the LIL beam at different intensities. Two kinds of fibers (500 μm diameter) have already been tested: a quartz/fluorinated-quartz/polyurethane fiber and a quartz/sylastic fiber. Analysis is under way.

4.2 Prototypes built and tested.

The first Q-Cal prototype, called proto-1, was built and tested in 1991 by the CRN Strasbourg group. It is shown schematically Fig. 16. Its dimensions were $5 \times 5 \times 20\,\mathrm{cm}^3$ and it included 1500 Ensign-Bickford HCR fibers tilted at 45° with respect to the beam, embedded in a lead matrix[3)] with a silica to lead volume ratio of 0.25. The calorimeter was longitudinally segmented in two halves read out independently by Philips 2020/Q PMTs (whose response is sensitive to UV light).

[2)] Produced by Ensign-Bickford, USA.

[3)] The lead sheets were provided by the RD25 Collaboration.

The response to 10 and 30 GeV electrons is shown in Fig. 17. We found some 10 photo-electrons per GeV and an electromagnetic energy resolution $\sigma/E = 24\%/\sqrt{E}+3\%$. Although far too short for hadronic calorimetry, this 1λ deep prototype was then tested with a 200 GeV/n sulfur beam in order to check the validity of the fiber response simulation program. Three measurements were made: without pre-radiator, behind 4 cm of tungsten (1λ) and behind 8 cm of tungsten (2λ). The results and the comparison with the simulation program are shown in Fig. 18. The light output normalization was fitted once for all configurations. It can be noted that the agreement is good, and that it improves for the later stages of the shower development. This result is very important because it validated our Monte-Carlo simulations of hadronic showers that otherwise are a very sensitive issue: the disagreements between calculations and measurements can be very large as a result of incorrect parameter tuning. In our case, this problem was even more delicate because heavy ion induced showers contain fragments whose behavior had to be treated independently of GEANT (FRITIOF plus a coalescence model to create the fragments[13]). Also in this test we had the occasion to check the pulse duration: at the ADC input, it was 10 ns wide at the base line.

The second prototype, called proto-2, is a very coarse hadronic calorimeter built and tested in 1992 as a first prototype for the Zero Degree Calorimeter of experiment NA50, by the INFN Torino and CRN Strasbourg groups. We knew from proto-1 that the agreement of the response with the simulation was good. The investigation concerned the hadronic energy resolution. The dimensions were $22 \times 22 \times 90\,\mathrm{cm}^3$, sufficient for longitudinal containment of 90% of the visible part of the hadronic showers. It was longitudinally segmented into four blocks each read out by four PMTs. Figure 19 shows a sketch of proto-2. The fibers were arranged inside the lead in four interleaved rectangular matrices, as shown in Fig. 20, with each matrix read out by a separate PMT. The total fiber-to-lead filling ratio was was 1/10; by analyzing the response of different combinations of PMTs, we could check the resolution for a volume ratio of 1/40, 1/20, 1/13.3 and 1/10. Also, different PMT combinations allowed us to check different fiber distributions. The fibers embedded in the lead were silica fibers with a numerical aperture of 0.37. To reduce cost, the connection between the quartz fibers and the PMTs was made with plastic fibers. The PMTs had ordinary glass window and type S photocathodes, so all UV light was lost.

Fig. 21 shows the obtained resolution compared with simulations. With 2 PM per block, we have two possible fiber orientations: the best resolution is attained when the fiber distribution approaches layers in the transverse direction (better sampling of the density profile of particles in the shower). The fitted energy resolution was on the order of $100\%/\sqrt{E}$.

To measure the visible width of the hadronic showers, a scan through the edge of the calorimeter was performed with 160 GeV protons[4]. Figure 22 shows the result and a comparison with simulations. The transverse, visible, hadronic shower size is almost an order of magnitude smaller than in conventional calorimeters: the calorimeter essentially works as a shower core detector. That is, only the rapidly moving and not significantly scattered particles of the shower core are sampled. One of the consequences is that the energy of a hadronic shower can be reliably measured, with good shower containment, as close as 2 cm from the calorimeter edge.

[4] Lead was placed at the calorimeter edge in order to let the shower develop uniformly.

The third prototype, called proto-3, was built and tested a few months ago in the framework of the quartz fiber calorimeter program financed by INFN, Italy (CPF2 Experiment). Its outer dimensions are $5 \times 5 \times 20\,\mathrm{cm}^3$. The main aims were to test a new arrangement of fibers inside the lead and to carefully measure the electromagnetic shower size. The calorimeter was laterally divided into independent readout channels. The fibers[5], still at 45° with respect to the incident particle direction, have 0.5 mm diameter, numerical aperture = 0.37, PMMA cladding and they touch each other in the transverse direction. The fiber planes are separated by 3 mm flat lead sheets. This arrangement was thoroughly studied with simulations and found to improve the energy resolution over the staggered arrangement. The fiber-to-lead volume ratio is about 1/7. The same fibers carry the signal to the PMTs of the Philips 2020/Q type (i.e. the readout of this calorimeter is sensitive to UV light).

Figure 23 shows the results of a scan with 8 GeV electrons through the edge of the calorimeter[6]. Only the response of one PM is shown. Figure 24 gives the electromagnetic lateral shower profile derived from Fig. 23. The results from the simulation are superimposed on the data in Fig. 23. The electromagnetic lateral shower profile can be fitted as a sum of two gaussian functions, with $\sigma = 0.86$ mm and 3.4 mm, with the two curves having approximately the same integral. The line response to 8 GeV electrons hitting the centre of one half module (right) is shown in Fig. 25 to be gaussian. Figure 26 shows the resolution as a function of the electron energy. A fit to the data points gives: $\sigma/E = (35.8 \pm 1.8)\%/\sqrt{E} + (-0.40 \pm 0.80)\%$ for the right PM and $\sigma/E = (37.9 \pm 2.1)\%/\sqrt{E} + (-0.01 \pm 0.90)\%$ for the left PM. This result shows that having the fiber distribution matching the shower profile makes the constant term in the energy resolution vanish.

The fourth prototype (see Fig. 27) of $4 \times 12 \times 30$ cm^3 size is being built at ITEP. The prototype will be assembled as a stack of 2 mm thick copper sheets (width 4.05 cm, length 30 cm). The copper sheets will be interspersed with thin layers of 420 μm diameter quartz fibers (core diameter 300 μm). The quartz fibers within each layer will be installed side by side as in Proto-3. The volume sampling fraction of such prototype is about 8%. Tests will be carried out at ITEP using a 5 GeV electron beam. The aim is to measure light yield and electromagnetic transverse shower profiles as a function of fiber orientation with respect to the beam. It is also important to check the simulation programs for a scenario in which a copper absorber is used.

4.3 Other applications of Q-Cal calorimeters in present and future experiments.

The Q-Cal original idea was intended to solve the problem of the zero-degree calorimeter for the NA50 heavy-ions experiment [21]. The NA50 zero-degree calorimeter is not yet finalized but the principle design has been approved by the SPSC and by the funding agencies. It is conceptually simple because the only requirements are radiation resistance and speed. As all of the particles it has to measure fall at the same spot, there is no need for spatial recognition.

---

[5] Produced by CeramOptec GmbH, Bonn, Germany.

[6] Note that the lead plates extended 2 cm laterally beyond the edge of the fiber planes. The resulting effect was that the shower developed in the same manner on both sides of the edge.

ALICE is proposing zero degree calorimeters to measure the spectator neutrons and protons through a design based on the Q-Cal concept.

RHIC has accepted the principle to mount zero-degree calorimeters at all of its intersections to be used to control the luminosity by measuring the spectator neutron flux. These calorimeters will be placed inside the magnets bringing the beams together. Furthermore, at its main experiments: BRAHMS, PHOENIX AND STAR, a study is under way to use these calorimeters, on an event-to-event basis, as centrality triggers. At heavy ions colliders, the stakes are much higher than at NA50 because of the beam pipes. Calorimetry coverage will be needed outside the beam pipes if it is found to be necessary to also measure the spectator protons (in addition to the neutrons). Also, the calorimeter may have to be retractable to a position at least 5 cm from the beam axis during injection. In these experiments the small shower size and the simplicity of construction will be of paramount importance. The fact that the Q-Cal can operate in high vacuum is also very important to all beam-pipe and total-containment calorimetry experiments.

As a spin-off from this development program a beam profile monitor based on a single layer of independently readout quartz fibers is being developed for use in LIL. This detector will be capable of measuring the beam shape of electrons and positrons on a pulse-by-pulse basis. Because of the absence of saturation of Cherenkov light, this detector will also yield a precision beam intensity monitor. An external detector is under construction, fully in-vacuum versions are possible and will be considered later.

4.4 What is known about silica fibers.

Large diameter ($> 100\mu$m) step index silica fibers come into three large categories: sylastic cladding, plastic cladding (relatively cheap) and fluorine-doped silica cladding (a few times more expensive). All of them are used primarily for military and medical purposes. They are also used mostly in the visible to infrared wavelengths while our needs are primarily in the UV and visible parts of the spectrum. This will entail a different cladding design, thinner than for infrared, hence, in principle, less expensive[7].

Outside the cladding, a buffer, or coating, is needed to protect the fiber, especially against water and cladding abrasion. The coatings come in different kinds (teflon, polyurethane, silicone, polyamide, aluminium, gold) and thicknesses. Most commercial coatings are designed for field handling and as a consequence are quite bulky. Heavy coating is useless and noxious in a calorimeter. Thin coatings or no coating (with thicker cladding) will be used in Q-Cals.

The numerical aperture ($\sqrt{n_1^2 - n_2^2}$) is generally 0.22 (maximum total reflection angle = 8.4°) for fluorine doped silica cladding, 0.37 (maximum total reflection angle = 14.2°) for plastic (fluorine-doped PMMA) cladding, and 0.5 to 0.6 for sylastic-clad fibers.

On top of what we have measured (Fig. 15), there is still a lot to learn about radiation hardness, especially in the photon-rich UV light domain. Moreover, most of the classical studies on radiation hardness are made with a small irradiation over a long length of fiber. In our case, the irradiation gradient is along η (i.e. the radius), roughly following the η dependence of the particles emitted by minimum bias events and there is a drop by a factor

[7] Most of the cost for fluorinated quartz fibers comes as a result of the cladding thickness.

of ten per unit of rapidity. The fibers, being at 45°, receive their maximum irradiation at the tips. To mimic the real irradiation the fibers should be irradiated very locally, on a length of 20 cm, and a background dose a factor 10 lower should be applied to the rest of the fiber. Then the fiber, which maximum length is only 3 m, should be tested with real particles at 45° degrees, for the Cherenkov light excites modes and a frequency spectrum which are difficult to reproduce with external light sources. The photodetector should be the same as foreseen for the VFC to ensure the correct wavelength sensitivity. For this reason, all existing measurements are not very relevant for our case.

If the radiation damage was to turn out to come mainly from the cladding, then large diameter fibers would be favoured.

Different numerical apertures also mean a different number of detected photons. We have tested a few plastic clad fibers at the PS with 8 GeV electrons. The fibers were at 45° with respect to the beam. The photo detector was a quartz-window Hybrid PhotoDiode (HPD) with a good single photoelectron resolution. The results are shown Fig. 28. A global fit to the spectra, taking into account the fake triggers and the fiber cross section, yields the number of p.e. per crossing. The result is 1.2 p.e. for the 0.6 mm diameter CeramOptec fiber (plastic clad). This has driven the choice of 500 μm diameter fibers [8] for proto-3 (see section 4.2).

We have also validated our computations of the Cherenkov effect (shown in Fig. 11) during the same beam test. Figure 29 compares the measured data with the simulated behaviour of the light output as a function of the incident angle.

4.5 Photodetectors.

Particular care has to be taken in the choice of the photon detectors. In fact, the Q-Cal resolution is limited by photon statistics. Every improvement in the photon detector effective quantum efficiency directly improves the calorimeter resolution, or, given a target resolution, allows the use of a smaller quartz fiber filling fraction and, consequently, a lower detector cost. It is therefore of paramount importance to use the highest quality photocathodes coupled to the most efficient photoelectrons collection system. Most of the Cherenkov light is emitted in the UV part of the spectrum, with a cut off given only by the quartz fiber cut off. It is then necessary to use quartz window photodetectors.

Moreover, the small Q-Cal shower dimensions require a fine readout segmentation, which, in turn, requires either pixelized detectors or many very small ones.

These considerations drove us to the choice of Hybrid PhotoDiode tubes (HPDs) [22] for the readout. These new photodetectors were developed thanks to a 5-years program financed by the LAA Project and then by a joint venture between INFN and Delft Electronische Producten (DEP) (see Fig. 30).

The main advantages of the HPD for Q-Cal are briefly summarized in the following:

a) The HPDs' photocathodes are built with transfer technology, which means that the photocathode can be much more sophisticated than what is possible with in-tube pro-

[8] It was decided, as a rule of thumb, that this prototype should consist of fibers which produce, on average, one photoelectron per particle crossing in a fiber. Future MonteCarlo will be necessary to examine, in detail, the detector characteristics of efficiency and resolution as a function of sampling fractions and fiber diameters used.

cessing. Also, the transfer technology allows the use of quartz windows at a negligible additional cost compared with glass windows.

b) The HPDs have very good single electron response and photon counting capabilities which are important in this detector.

c) The HPD is easily pixelizable. A 25 mm diameter, 7-pixels version has been chosen to minimize the number of tubes and the connection length[9].

d) Most important, the HPDs have an optimal photoelectron utilization efficiency. While, in a PMT, many of the photoelectrons miss the first dynode, an HPD has virtually 100% collection efficiency. This gives the HPDs an advantage over all known PMTs [23].
In principle, PIN diodes or Avalanche PhotoDiodes (APD) have an even better effective quantum efficiency, but the PIN diode capacitance noise and the APD "excess" noise and sensitivity to highly ionizing particles [24] more than offset this advantage.

e) The photodetector needs to be fast and proper versions of the HPD (cross focussed ones) have demonstrated to be sufficiently so (< 1.5 ns raise and fall times [22]). For the hadronic prototype we intend to build (see section 7), a temporary compromise was made in the choice of HPD.
The quartz window must be thin in order to minimize the pixel-to-pixel optical cross-talk. The fast cross focussed HPDs require a spherical photocathode. A suitable thin, spherical quartz window, although straightforward has not yet been engineered. For this reason, we fell back on thin flat windows and, therefore, on proximity focussed tubes. Because of the larger silicon pixel surface, the large capacity induces slow (~ 5 ns) rise times. Despite their slow rise time, these tubes were measured to yield 100 ps timing capabilities with on the order of one hundred photoelectrons.

5 DESCRIPTION OF A POSSIBLE VFC FOR A MULTI-TeV EXPERIMENT.

5.1 The basic geometry and its simulation.

The MonteCarlo calculations indicate that the best results, with respect to resolution, shower size and light yield, are obtained when there is an angle of 45° between the shower and the fiber axis. This requirement makes the precise localization of the shower position in an $\eta - \phi$ coordinate system non-trivial because, unless timing is taken into consideration, the response of this calorimeter is independent of the hit position along the fibers.

To circumvent this problem, the first design that we studied is shown in Fig. 31. The detector is divided into eight octants in ϕ and each resulting trapezoid is inclined with respect to the beam by an angle of 50°. As the forward calorimeters cover a pseudorapidity interval between 2.5 and 5 units, (i.e. between 0.77° and 9.4°), the particles with $\eta = 2.5$ will enter the calorimeter with an incident angle of 40°, while for the particles next to the beam pipe the angle will be 50° (in the range $40 \div 50°$ the difference of the mean responses is less than 0.5% as shown in Fig. 32).

The fibers lay in planes parallel to the front face of the trapezoidal triangles and in

[9] If the fibers that must carry the signal from the calorimeter to the photon detector are too long, their cost can be comparable to that of the photodetectors themselves. Also, connecting too many fibers on a single tube may be cumbersome.

alternate layers they are parallel to the left and to the right side of the trapezoid. "Left" and "right" layers are read out independently. The fibers from each orientation can be further regrouped laterally (and longitudinally) and coupled to separate photo detector pixels (see Fig. 33). The fine lateral segmentation allows a precise shower positioning via the center of weight method. The longitudinal segmentation permits discrimination of the electromagnetic and hadronic showers as well as the minimization of the total pulse duration. Note that the calorimeter is so fast that the pulse duration is otherwise dominated by the shower dimensions (1.5 m in length) times the spread of the light velocity in the fibers (20 ± 1 cm/ns).

This division gives a kind of a matrix where left and right fibers give two coordinates of the position of the incoming particle, similar to the approach applied in stereo MWPCs (see Fig. 33d). The determination of the shower position is derived from its position in the local "left-right" coordinate systems of the each octant and the precision is determined by the size of the modules. Timing may be used to resolve ambiguities. Jets would be similarly treated as hit clusters.

The geometry was simulated with a MonteCarlo program. The dimensions of the calorimeter were chosen in such a way that the front face could be positioned at a hypothetical distance of 11 m from the interaction point. The outer radius was 2.2 m enabling a good lateral hadronic shower containment for $\eta = 2.5$ particles, its length was 3 m (largely overestimated, 1.5 m turned out to be quite enough), and the radius of the inner (conical) hole which accommodates the beam pipe was 14.7 cm at the beginning and its angular opening was equal to 0.77° (corresponding to $\eta = 5$). The width of the modules was chosen to be 4 cm (in future calculations it will be reduced to 1 cm to take full advantage of the narrowness of the showers). The fiber to lead volume ratio was chosen to be equal to 1/10.

5.2 The computed response.

A jet was simulated (with PYTHIA [2]) together with 30 minimum bias events as shown in Fig. 34. An example of the response of the calorimeter is shown in Fig. 35. The simulated jet was positioned at an unfavorable position, i.e. close to an edge of octant 4 (4th octant clockwise starting at top of Fig. 35), and at $\eta = 3$. The fibers hit by the jet also collect the signal from particles from minimum bias events at higher rapidities . The jet position is well visible, against the background, in the "right" coordinate, but less visible in the "left" coordinate. The confusion region is limited to the 4 or 5 segments reaching to rapidities higher than 4.5. However, the confusion region is geometrically quite narrow and even this simulated detector geometry can give a reasonable position resolution with an angular acceptance as deep as $\eta = 5$. This problem of confusion is fully solved in a different geometry described later. If we assume that the error in determination of the jet position in the left/right system of each octant is one segmentation unit (4 cm), resolutions $\Delta\eta = 0.2$ for $\eta = 5$, and $\Delta\eta = 0.02$ for $\eta = 2.5$ are obtained. The resolution in ϕ is $\Delta\phi = 0.27$ for $\eta = 5$, and $\Delta\phi = 0.02$ for $\eta = 2.5$. Even in the worst possible case, for $\eta = 5$, the spatial resolution defined as $\Delta R = \sqrt{\Delta\eta^2 + \Delta\phi^2}$ is equal to 0.34. With the center of weight method or finer segmentation the resolution will further improve.

5.3 The problem of the minimum bias at high rapidity.

The fluctuations of the energy deposited in the modules by minimum-bias events can deteriorate both the position and the energy resolution of the calorimeter. The first three segments, reaching next to the beam pipe, are continuously illuminated by particles produced in minimum bias events. These modules are therefore subject to the large fluctuations of the integrated response. Because of this partial pile-up there is a loss of contrast for jet signals. Moreover, the fluctuations of the response in strongly illuminated modules can deteriorate the energy resolution or even fake jets. There are several ways to solve this problem, including stepping the calorimeter in rapidity (see next section), time slicing and possibly introducing an additional plane of fibers.

5.4 The proposed VFC geometry.

The easy way to decrease the influence of the heavily illuminated modules on the position and energy resolution of the calorimeter would be to decrease the rapidity acceptance of the calorimeter. Figure 36 shows the response curves for the left and right modules of the octant containing the jet for different rapidity acceptances. If the calorimeter is restricted to the pseudorapidity region up to $\eta = 4.5$, the response due to minimum bias events decreases considerably. When the limit is set to $\eta = 4$, the background becomes negligible. This leads to an interesting idea of minimization of the background without decreasing the acceptance: a division of the calorimeter in segments corresponding to a rather crude binning in pseudorapidity. Figure 37 shows a longitudinal cross section of one octant. The calorimeter is divided in rings each covering $\Delta\eta = 0.5$[10]. Each ring is displaced by 40 cm in z. The responses from deeper segments mix only after the lower rapidity hadronic showers pass through the maximum. As can be seen from Fig. 13 and taking into account that one third the energy in a jet is electromagnetic, more than 75% of the signal is deposited in the first layer, which does not receive contributions from higher rapidities.

Since the position of the lower rapidity showers is determined before they mix their signal with the higher rapidity showers, their tail can be easily followed (uncontaminated by higher η contributions) in at least one projection. For the deepest reaching modules ($\eta > 4.5$), time slicing or the addition of a third layer of fibers may be necessary in order to resolve ambiguities. $\eta > 4.5$ would radically solve the problem.

As for time slicing, it can be effective to determine a shower rapidity but it is limited by the primary vertex indetermination, i.e. with a resolution of < 10 cm along the fibers (see also section 5.5).

An additional possibility is to build a calorimeter with fibers at 45° down to rapidity 4 or 4.5 and make up the balance with a spaghetti-type (quartz fibers nearly parallel to the incoming particle direction) quartz calorimeter. This last geometry is less sensitive to the shower core and is essentially sensitive only to the randomized part of the electromagnetic components of the shower which happen to be oriented within the fiber acceptance cone. This choice will result into a higher systematic error in the energy resolution and in a 5-fold loss of light production. However, energy resolution is less important at these high rapidities and the loss in light production is well compensated for by the higher minimum shower

[10] The dimensions of the stepping is not yet optimized.

signal. In addition such a tower structure insert (possibly using types of fiber and absorber which are different[11] from the bulk of the VFC) would be introduced just in the place where minimum bias pileup would make reconstruction difficult in the 45° configuration (the bulk of the background would then be removed from the higher precision sections of Q-Cal).

Added advantages from this configuration also include the fact that the detector would be shortened and that the insert could be extracted, independently from the rest of the VFC, allowing removal of the most radio-activated detector component and easier access to the beam pipe.

All of these options must be thoroughly simulated and, if necessary, prototyped and beam tested.

5.5 How to make a simple E_T trigger.

It is evident from Fig. 37 that an E_T trigger with a granularity $\Delta\eta = 0.5$ can be trivially obtained by independent readout of the different rapidity rings, as 75% of the energy of jets is deposited in the first 2λ of the calorimeter. The performances of finer steppings have yet to be studied. Very likely, it will be advantageous to synchronize the stepping with the longitudinal readout segmentation. Note also that in a jet the longitudinal shower fluctuations will be depressed by a factor equal to the square root of the number of particles. Hence, the incomplete shower collection in the first step should be of no consequence.

The temporal distribution of the response can also be turned into a more precise E_T trigger. As the Cherenkov effect is instantaneous and the small capturing angle of the quartz fibers limits the speed of the photon propagation in the fibers to the interval between 19 and 21 cm/ns, the temporal distribution of the responses within a single octant can give fast information about the pseudorapidity of the particle producing the shower. The longitudinal distribution of the primary vertices has a dispersion $\sigma_z = 5.5$ cm, corresponding to 180 ps. Assuming a time resolution of the fibers and their photodetector of 100 ps, the radial resolution is on the order of 6 cm, i.e. about 0.3 units of rapidity at $\eta = 5$ and less than 0.1 at $\eta = 3.5$.

5.6 The Q-Cal in an LHC experimental hall.

This calorimeter can easily fit within the space constraints of the main experiments proposed thus far for LHC. Furthermore, the photodetectors are in an easily accessible and well shielded position. Finally, the Q-Cal is chemically and radiochemically inert, it has no liquid or gaseous component, it is easy to disassemble under remote control in the case of servicing to other detectors (its activation will depend on the absorbing material; in the case of lead it will present on the order of 20 mSv/h after 30 days of irradiation time [6]), and it is expected to be nearly maintenance-free.

6 WHAT WE NEED TO LEARN.

6.1 Fibers.

The main requirements for the fibers are the following:

[11] Higher grade quartz fibers and tungsten absorber, which are more expensive than other options, might be feasible here.

a) radiation resistance,
b) largest possible transmittance window possibly extending up to the UV quartz cut-off,
c) large numerical aperture to increase the light yield and decrease the sampling fraction (i.e. the cost),
d) small numerical aperture to contain the visible shower dimensions (and to maintain good time resolution),
e) sufficient mechanical flexibility to allow easy assembly (i.e. small diameter).

Obviously, requirements (c) and (d) are in contradiction. However there is ample working space between the two requirements and, most important, there are fibers that happen to be in that range. Some contradiction may also exist between requirements (a) and (b) as there are indications that the transparency in the UV region is degraded by irradiation more than at larger wavelengths [25].

Clearly, the best choice of fiber technology and diameter can only be made after careful investigation of the many parameters involved.

Some of the items that need to be studied are:

- the core behaviour under irradiation at different wavelengths for different impurities and OH content,
- the influence of cladding material and thickness on the fiber behaviour,
- the response to single, superluminal particles of all possible fibers,
- the best protocol to make radiation damage studies with different sources: ^{60}Co, low energy (MeV) electrons, charged hadrons, neutrons and with showers at the LIL,
- characteristics of the calorimeter as a function of fiber diameter and fiber arrangement inside the absorber (to be studied via MonteCarlo simulations and small prototypes).

6.2 Absorber.

Our present best choice for the absorber is lead, for it has a low induced radioactivity, it is cheap and it can be machined easily. Still, the bulk of its radioactivity comes from impurities. A study on the subject started by RD25 needs to be continued and extended to other metals.

For certain applications, it could be necessary to have shorter showers. For this purpose, we have to study tungsten and its derivative, the copper-bound syntered tungsten powder. On the other hand, it could be advantageous in some cases to have a large Moliere radius, so we have also to study copper and iron absorbers.

6.3 Photodetectors.

The choice of proximity focussed HPDs is adequate for the needs of this R&D project. The price of about 400 CHF/pixel for an highly UV sensitive device is also quite competitive. However, in view of the application to a VFC, its speed should be improved.

The development of a spherical-spherical quartz window for the cross focussed version will be pursued in parallel.

A special air Winston cone honeycomb which allows a larger surface of fibers to be focussed on a smaller photocathode surface without pixel-to-pixel cross-talk will also be studied along with other focussing methods.

The HPD readout will be made, at least in a first phase, with fast charge amplifiers developed by J.C. Santiard in the framework of the LAA Project. This amplifier matches well the present speed of the proximity focussed HPD. Faster current amplifiers will be tried on faster HPD models.

Concerning radiation hardness, the HPD silicon chip is a simple depleted silicon diode and it is not expected to be particularly sensitive to irradiation. Radiation load is expected to increase the leakage current which will be, at least in first approximation, of little effect to AC-coupled amplifiers. Tests will be done to check the leakage current influence on the noise, which is expected to be small compared to the physics noise from minimum bias events. More care has to be put in the construction of the amplifiers that can easily be more sensitive to irradiation than the HPD chip. However, it is to be noted that, thanks to the Q-Cal geometry, the HPDs and the amplifiers will sit in a well shielded location.

Final goals, with respect to the HPD, also include larger photocathode sensitive areas with more pixels for reduced prices. The PHASE laboratory should play a key role in that domain[12].

Standard PMTs are not completely forgotten. Tests on commercial small PMTs has already started. Of particular interest are the soon to be commercialized 5600-series HAMAMATSU tubes [26], if they prove to have a good photoelectron collection efficiency and an improved photocathode UV quantum efficiency. Tests of these tubes are scheduled for January 1994.

6.4 How to make a VFC.

The following are some of the questions that will be answered through the construction of a hadron prototype:

- What is the best longitudinal segmentation and rapidity stepping?
- What is the best transverse size for a module?
- What is the hadronic energy resolution in different configurations?
- What is the spatial (η-ϕ) resolution for hadrons in different configurations?
- What is the e/h ratio in these configurations?
- How to built such a device in a self-supporting structure?
- How to best organize the fibers on the photodetectors?
- Which is the best read-out algorithm?

7 THE R&D PROGRAM.

7.1 Prototypes.

Some small EM prototypes will have to be built for specific purposes. For instance, to measure the transverse shape of a shower when using fibers with different numerical apertures.

The biggest effort consists in building a 150 cm long hadron prototype. Seen from the front (see Figure 38), it will look like a shortened (Δr = 20 cm) octant with a ϕ aperture of 22.5° as the actual future VFC. It will have fibers in layers with 2 orientations, divided in 1 cm wide lateral segments. A structural plan is being drawn. Longitudinally, the prototype will

[12] PHASE constructed the first HPD in 1962 and patented the result.

be divided into separate modules. Shifting modules vertically will allow to test the stepping geometry.

Different modules may be built with different fiber filling. Reordering the sequence of the different modules in the beam line will allow the cross-evaluation of different types of fiber. In the case that the fourth small prototype (Proto-4) would yield particularly good results in beam tests, parallel construction of a 0° hadronic calorimeter will be considered.

7.2 Fibers.

A thorough study of the different parameters (core, cladding, buffer, diameter,...) by comparing beam tests with optical tests and simulations is proposed. The beam tests would be done on single fibers and on calorimeter prototypes, with electrons and hadrons at the CERN PS, SPS, LIL and at ITEP. Irradiation of single fibers and calorimeter prototypes would be done at CERN LIL with 500 MeV electrons, CERN ACOL with hadrons, GANIL with 100 MeV/n oxygen ions, Vivirad in Strasbourg with 2 MeV electrons and reactors in Pavia and Strasbourg with reactor neutrons.

Studies on radiation damage will also be performed at ITEP for different kinds of quartz fibers in the dose range from 10 MRad to 10 GRad. The attenuation lengths will be measured in the wavelength range from 200 to 800 nm. In addition, possible annealing with time will be studied.

7.3 Absorber.

Different absorbers (lead, copper, iron, sintered tungsten) are going to be beam tested and irradiated. Particular attention will be paid to their activation properties.

7.4 Photodetectors.

A program is starting at the PHASE laboratory to finalize the HPD design to our needs. It will focus mainly on the silicon chip and its readout chain. The light collection, from the fiber to the photocathode of the HPD will also be specifically studied. PMTs will not be forgotten: a dedicated study of the available quartz-window small tubes will be undertaken.

7.5 Software development.

A large effort will be done in two directions:

- Continuation of the simulations. In particular:
  - Simulations of how the calorimeters work. We will introduce multiple scattering and interactions in the fibers.
  - Event simulations to keep close to the physics.
  - Full detector simulation: we will introduce our VFCs in the presently proposed LHC apparatus to see how they match the rest of the detector.
- Write and implement the algorithm that reads the VFC more powerful.

7.6 Time scale.

Table I below gives the time scale of the different items under study in the R&D program.

Table I. Time scale.	
Fiber testing and irradiation tests	Non stop until end of 1995
EM Prototypes	2 in 1994 and 2 in 1995
Hadron prototype	Start in may 1994 Finish construction in august 1994 Tests until end of 1995

8 BUDGET AND SHARING OF RESPONSIBILITIES.

Tables II and III below summarize the budget requested to perform the R&D program outlined in the previous section and the division of responsibility between the members of the collaboration, respectively.

Table II. Budget.		
Tests of fibers		
	fibers	20 kCHF
	photodetectors	10 kCHF
	irradiation facilities	25 kCHF
	mechanics	10 kCHF
SUBTOTAL		65 kCHF
Photodetector program		
	HPD	20 kCHF
	Silicon wafers	20 kCHF
	Optical components	10 kCHF
	Amplifiers+PC boards	20 kCHF
SUBTOTAL		70 kCHF
Prototypes		
EM prototypes (4×)		
	Fibers	20 kCHF
	Absorber	5 kCHF
	photodetectors	5 kCHF
	mechanics	5 kCHF
	electronics	10 kCHF
Hadron prototype		
	fibers (90 km, ϕ=500 μm)	250 kCHF*
	Absorber	10 kCHF
	Photodetectors (50)	150 kCHF**
	mechanics	10 kCHF
	electronics	50 kCHF
SUBTOTAL		515 kCHF
TOTAL		650 kCHF
CONTINGENCY (10%)		60 kCHF
GRAND TOTAL		710 kCHF

*) partly provided by ITEP.
**) provided by the LAA Project.

Table III. Sharing of responsibility.	
Fibers irradiation	CERN, CRN, ITEP, FSU, Pavia and Torino
Fibers testing	Bologna, CERN and ITEP
Simulations	Bologna, CRN, CERN, FSU and ITEP
Photodetectors, HPDs	PHASE, Pavia and CERN
Proto construction and tests	Bologna, CERN, CRN, ITEP and Torino

9 CONCLUSIONS AND R&D REQUESTS.

The technique described in this proposal is well adapted to the needs of very forward calorimetry at LHC. Calorimeters with amorphous silica ("quartz") fibers as active material are highly radiation resistant and fast. They produce sufficient energy resolution from visible shower sizes a factor ten smaller than other, conventional, calorimeter techniques. They are insensitive to radio-activation and to low energy neutrons, and they do not show, in principle, pulse height saturation or rate effects.

Scope of the R&D program presented here is to identify the components of the future very forward calorimeter, thus bringing this still very young technology into a mature stage.

We ask the Detector Research and Development Committee the approval of this proposal and of the support indicated in Table IV.

Table IV. Support requested to CERN.		
BEAM TIME		
Fibers irradiation	LIL	1 month of parasitic beam time integrated over 1994 same for 1995
	ACOL	Possibility of exposing fibers in the vicinity of the antiproton production target
Fibers testing	PS	5 periods of 5 days in 1994 5 periods of 5 days in 1995
Prototypes testing	SPS	2 periods of 10 days in 1994 3 periods of 10 days in 1995
ELECTRONIC POOL	CERN Electronics Contrib. (CEC) of 100 kCHF	
COMPUTER TIME	50 hours (1994) and 50 hours (1995) mainly for simulations on CERNVM. 1000 hours of CSF.	
CONTRIBUTION TO THE GENERAL BUDGET	100 kCHF	
SUPPORT TO EASTERN EUROPE COLLABORATORS	6÷9 months in 1994 and 6÷9 months in 1995 to cover living expenses at CERN	

References

[1] P.T. Cox et al., Proceedings of the "Large Hadron Collider Workshop", Aachen 4-9 October 1990, CERN 90-10, Volume II, p. 50.

[2] PYTHIA: H.-U.Bengtsson and T.Sjöstrand, Computer Physics Commun. 46 (1987) 43.
JETSET: T.Sjöstrand, Computer Physics Commun. 39 (1986) 347,
T.Sjöstrand and M.Bengtsson, Computer Physics Commun. 43 (1987) 367.

[3] see, for example, J. Colas et al, Proceedings of the "Large Hadron Collider Workshop", Aachen 4-9 October 1990, CERN 90-10, Volume I, p. 370.

[4] see, for example, C. Albajar et al, Proceedings of the "Large Hadron Collider Workshop", Aachen 4-9 October 1990, CERN 90-10, Volume II, p. 621.

[5] M.H. Seymour, Proceedings of the "Large Hadron Collider Workshop", Aachen, FRG, 4-9 October 1990, CERN 90-10, Volume II, p. 557.

[6] G. Stevenson, Proceedings of the "Large Hadron Collider Workshop", Aachen 4-9 October 1990, CERN 90-10, volume III, pp. 302 and 566.
A. Ferrari, private communication and communications at CMS and ATLAS meetings.
G. Anzivino et al.,"Effects of induced radioactivity in very forward calorimetry, a comparison between different techniques", *To be published in proceedings of the IV International Conference on Calorimetry in High Energy Physics*, Isola d'Elba, Italy, 1993.

[7] A.P.T. Palounek et al., SDC Solenoidal detector notes, SDC-93-467.
L.S. Waters et al., SDC Solenoidal detector notes, SDC-92-361.
D.E. Groom, SDC Solenoidal detector notes,. SDC-91-122.

[8] A. Caldwell et al., NIM **A330** (1993) 389.

[9] ALICE LOI CERN/LHCC/93–16, LHCC/I 4, 1 March 1993.

[10] H. Gutbrod, private communication.
J.D. Bjorken and L. McLerran, Phys. Rev. D 31 (1985) 63.
A. Dumitru, L. McLerran, H. Stocker, W. Greiner, "Soft Photons at RHIC and LHC", UFTP preprint 340/1993, to be published in Phys. Lett. B.

[11] One of us (P. Gorodetzky) is involved in RHIC zero degree calorimeters.

[12] B. Grosdidier, thesis, University Louis Pasteur, Strasbourg, 1992.

[13] D. Lazic, thesis, University Louis Pasteur, Strasbourg, 1993.

[14] P. Gorodetzky, B. Grosdidier and D. Lazic, "Very Hard Radiation Resistant and Ultra-Fast Calorimetry", in *Radiation Physics and Chemistry*, (Pergamon Press, Oxford, U.K.) **41** nos. 1/2, (1992) p. 253, eds. R. Clough and K.F. Johnson.

[15] C. Baglin, A. Bussiere et al., "A New Concept Hadronic Sampling Calorimeter," *IEEE NSS*, Orlando, USA, 1992.

[16] G. Anzivino et al., "Quartz Fibers for Very Foward Calorimetry: Ultra-Fast, Infinitely Rad-Hard and Shower Core Sensitive", *To be published in proceedings of the IV International Conference on Calorimetry in High Energy Physics*, Isola d'Elba, Italy, 1993.

[17] G. Anzivino et al., "Effects of Induced Radioactivity in Very Forward Calorimetry, A Comparison Between Different Techniques", *To be published in proceedings of the IV International Conference on Calorimetry in High Energy Physics*, Isola d'Elba, Italy, 1993.

[18] E. Chiavassa et al., "The Zero Degree Hadron Sampling Calorimeter for the NA50 Experiment at the CERN PS", *To be published in proceedings of the IV International Conference on Calorimetry in High Energy Physics*, Isola d'Elba, Italy, 1993.

[19] G. Anzivino et al., "Design of a Quartz Fiber Calorimetry for a Collider Experiment", *To be published in proceedings of the IV International Conference on Calorimetry in High Energy Physics*, Isola d'Elba, Italy, 1993.

[20] H. Fabian, U. Grzesik and K.F. Klein, Proceedings of the "Large Hadron Collider Workshop", Aachen 4-9 October 1990, CERN 90-10, volume III, p. 736.
M. Tavlet, H. Beger and H. Schonbacher, Review on radiation effects in optical fibers, CERN internal report, TIS-RP/IR/SS-21, SPS/88-29(ARF), 21 June 1988.

[21] NA50 Collaboration Proposal for an experiment at SPS, CERN/SPLC 91-55 (1991)

[22] R. DeSalvo et al., NIM **A315** (1992) 375.
H. Arnaudon et al., CERN-PPE/93-101 and submitted to NIM.
G. Anzivino et al.,"Recent Developments of the HPD", *To be published in proceedings of the IV International Conference on Calorimetry in High Energy Physics*, Isola d'Elba, Italy, 1993.

[23] C.D'Ambrosio et al., CERN-PPE/93-140, to be submitted to NIM, 23 June 1993.
C.D'Ambrosio et al., CERN/LAA/SF/93-37, 29 November 1993.

[24] The silicon chip inside the HPDs will be just as sensitive as the PIN diode (but much less than the APD [27]) to highly ionizing radiation. However, due to the intrinsic and internal HPD gain, the effect of ionizing particles will be reduced by a factor of $2000 \div 3000$. Also, the cross focussed HPD will use smaller diodes (less than 10% of the photocathode area) and will then be even less sensitive to highly ionizing particles.

[25] A. Golutvin, private communication and Ensign-Bickford, USA technical data.

[26] Private communication and advanced information data sheet provided by HAMAMATSU.

[27] G. Anzivino et al., "Failure Modes of an Avalanche PhotoDiode", *To be published in proceedings of the IV International Conference on Calorimetry in High Energy Physics*, Isola d'Elba, Italy, 1993.

FIGURE CAPTIONS

Fig. 1 : (a) Hadronic shower size in $\Delta\eta$ as a function of η, for the calorimeter geometry sketched in (b). The hadronic showers size (at 95% collection efficiency) is assumed to be 25 cm. The dot-dashed line is the same for a detector with a Q-Cal as VFC.

Fig. 2 : a) Energy flow normalized to the primary parton energy as a function of the distance from the jet axis in $\Delta R = \sqrt{\Delta\eta^2 + \Delta\phi^2}$.
b) Integrated energy flow as a function of the distance from the jet axis, normalized to the jet total energy (jets as defined in the text).

Fig. 3 : Difference between reconstructed jet energy and primary parton energy, normalized to the latter (jets as defined in the text).

Fig. 4 : Particle density as a function of the radial distance from the jet axis (jets as defined in the text).

Fig. 5 : Missing transverse momentum distribution for the $H \rightarrow ZZ \rightarrow ee\nu\nu$ signal, from background from the ZZ continuum and from Z+jets events, for different calorimeter coverages in η (from [3]).

Fig. 6 : Rapidity distribution of the tagging jet (from [5]).

Fig. 7 : Energy flow as a function of η for a superposition of 40 minimum bias events.

Fig. 8 : Added term to the energy resolution due to overlapping minimum bias events (in the η range from $2 \div 5$) as a function of the jet p_T for two luminosities: $1.7 \times 10^{34}\,\mathrm{cm}^{-2}\,\mathrm{s}^{-1}$ (40 minimum bias events per crossing, lighter region) and $0.6 \times 10^{34}\,\mathrm{cm}^{-2}\,\mathrm{s}^{-1}$ (15 minimum bias events per crossing, darker region). Below $p_T = 200\,GeV$ the energy resolution will be dominated by fluctuations in the background.

Fig. 9 : Transparency of a 3 mm thick Suprasil silica disc, as a function of wavelength, after different doses of irradiation.

Fig. 10 : A schematic view of the Cherenkov effect in a step index optical fiber. A photon emitted in the point P along the Cherenkov cone hits the interface core-cladding at point A. See reference [13] for exact specifics of all the terminology show in the figure.
a) Three-dimensional view;
b) Zoomed view of the point of impact of a light ray on the interface core-cladding;
c) Projection into a plane perpendicular to the fiber axis.

Fig. 11 : Distribution of the number of photons that exit the fiber ($\phi = 1$ mm, NA = 0.37) as a function of the impact parameter, b, and the incident angle, α, of the particle trajectory for a $\beta = 1$ particle. Reflections from the front surface of the fiber are taken into account (no optical contact with a photo-detector). The wavelength distribution of the produced photons is multiplied by the "nominal" quantum efficiency of a Philip's 2020/Q photocathode.

Fig. 12 : Distribution of the number of photo-electrons detected by a nominal Philips 2020/Q photocathode for the same fiber than Fig. 11, as a function of α and of the velocity, β, of the particle.

Fig. 13 : Top: schematic view of the calorimeter. The calorimeter is subdivided, longitudinally, in slices. Each slice is connected to a PMT. Bottom: The simulated anode pulses of the first 6 PMTs for an oxygen ion (200 GeV/n). Each pulse is shifted by 1 ns in order to the shower development velocity. The total pulse is the sum of the 6 pulses, each of them delayed by one ns relative to the next one.

Fig. 14 : Linearity of the proposed NA50 zero degree calorimeter as computed by the simulation program. To convert the horizontal scale in GeV, one mass unity has to be multiplied by 160. Near each point is indicated the number of simulated events. The error bars correspond to the FWHM energy resolution as deduced from a least squares fit.

Fig. 15 : Light yield of silica fibers as a function of the dose.

Fig. 16 : Side view of Q-Cal proto-1.

Fig. 17 : Line shape responses of the first prototype to 10 and 30 GeV electrons.

Fig. 18 : Comparison between the measured (solid lines) and simulated (dashed lines) signal distributions of proto-1. Zero, four and eight cm of tungsten (0, 1, 2 interaction lengths) were put in front of the module. The beam was 200 GeV/n Sulphur ions. PM1 and PM2 readout the upstream and downstream half of the module respectively.

Fig. 19 : Lateral view of proto-2.

Fig. 20 : Distribution of the fibers in proto-2. The fibers within each block were connected to four different PMTs. By reading different combinations of the PMTs, the response of the calorimeter to different fiber densities and distributions could be obtained.

Fig. 21 : The measured (with S^{32} ions, 200 GeV/n) and calculated hadronic resolution for proto-2, as a function of the fiber density (i.e. number of PM per block). The large error bars for the simulated events arise from low statistics (only 100 events corresponding to 170 hours of CPU time on a IBM 3090). Experiment errors are inside of the data point markers. See text for the difference between the two different kind of data points.

Fig. 22 : Edge scan of proto-2 using 160 GeV protons. The solid line is the result of the simulation.

Fig. 23 : Edge scan of proto-3, measured using a CERN PS 8 GeV electron beam. The edge position is at $x = 2.2$ mm. The solid line is an arc tangent fit to the data.

Fig. 24 : Electromagnetic lateral shower profile in proto-3. The solid line is the result of the simulation.

Fig. 25 : Signal line shape of the response of proto-3 to 8 GeV electrons.

Fig. 26 : Resolution of proto-3 (circles and squares) as a function of the electron energy along with the data from proto-1 (triangles). Thanks to the improved fiber distribution scheme, the constant term of the fit for proto-3 is compatible with zero.

Fig. 27 : Schematic view of the fourth prototype. The insert shows the fiber arrangement.

Fig. 28 : Response of fibers with different diameters to 8 GeV electrons impinging at 45° with respect to the fiber axis. The fibers are viewed by a quartz window HPD.

The first peak (on the left of the histograms) corresponds to zero photoelectrons. It is the result of the inherent inefficiency of the fiber and of false triggers. A global fit to the spectrum was used to extract the number of p.e. for a 8 GeV electron passing through the center of the fiber (indicated in each figure).
(a) 200 μm diameter quartz/plastic fiber from CeramOptec.
(b) 300 μm diameter quartz/plastic fiber from CeramOptec.
(c) 600 μm diameter quartz/plastic fiber from CeramOptec.
(d) 300 μm diameter quartz/plastic fiber from CeramOptec (different preform than (b)).
(e) 1000 μm diameter quartz/plastic (HCR) fiber from Ensign-Bickford.

Fig. 29 : Comparison between the projection of Fig. 11 on the α-axis (full line) and the measured points for 1 mm HCR fiber (plastic clad). The simulations has been normalized to the data at 45°. At angles smaller then 30°, the beam particles begin to be directly seen by the photodetector.

Fig. 30 : Schematic view of the HPD: a) cross focussed; b) proximity focussed.

Fig. 31 : Geometry of a Q-Cal VFC under study:
a) 3-d view, b) longitudinal cross section, c) front view.

Fig. 32 : Response distribution of the VFC to showers as a function of the fiber tilt with respect to the beam. (Notice that Fig. 29 shows the response of individual fibers to individual particles.)

Fig. 33 : Arrangement of the fibers in the calorimeter. Fibers (not shown) are grouped in 4 cm wide strips within each layer (1 cm grouping would better match the narrow size of the showers). The next layer has a different fiber orientation, so the layers with "left" (a) and "right" (b) orientations are alternating. This gives a grid (c) where the coordinates of the hit modules give an information about the position of the shower. The correspondence with pseudorapidity intervals is shown in (d).

Fig. 34 : $\theta - \phi$ plot of the simulated jet with $\eta = 3$: a) energy of the electromagnetic and b) hadronic component of the jet, as a function of the angle with respect to the beam pipe (θ) and the azimuthal angle (ϕ), c) and d) are the same distributions with 30 minimum bias events superimposed.

Fig. 35 : Simulated response shape of the calorimeter to the same jet (seen in octant 4) as in Fig. 34. The distributions of the response for the two orientations are shown above each octant (one bin correspond to a 4 cm wide segment). The dark spot inside the calorimeter drawing shows the jet's placement (closer to octant 5 than octant 3).

Fig. 36 : Response distribution for the calorimeter with various acceptances. The confused jet response of octant 4 in Fig. 35 (also shown in Fig. 34) is detailed in this figure.

Fig. 37 : Longitudinal cross section of an octant with an altered design, showing the division of the calorimeter in steps corresponding to different η bins. The mixing of the responses from different η bins occurs only in later stages of the shower development, making the deconvolution of different showers easier.

Fig. 38 : Schematic front view of the proposed hadron prototype.

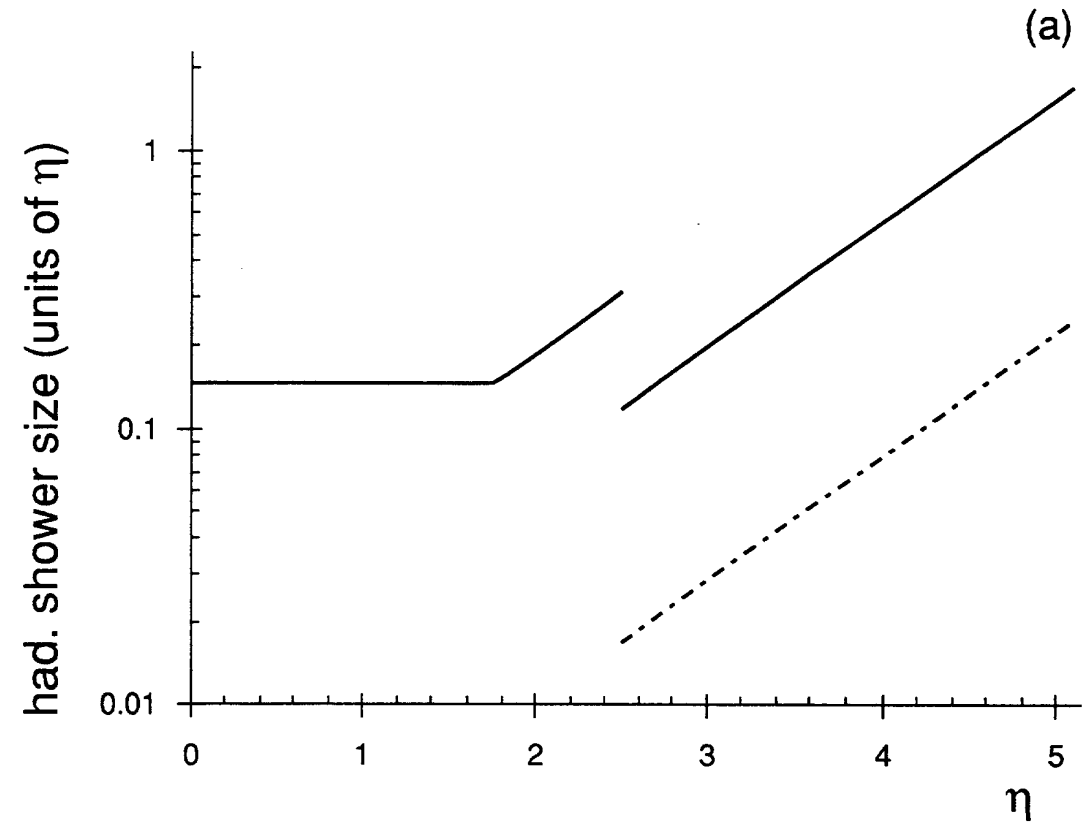
(a)
had. shower size (units of η)
1
0.1
0.01
0
1
2
3
4
5
η

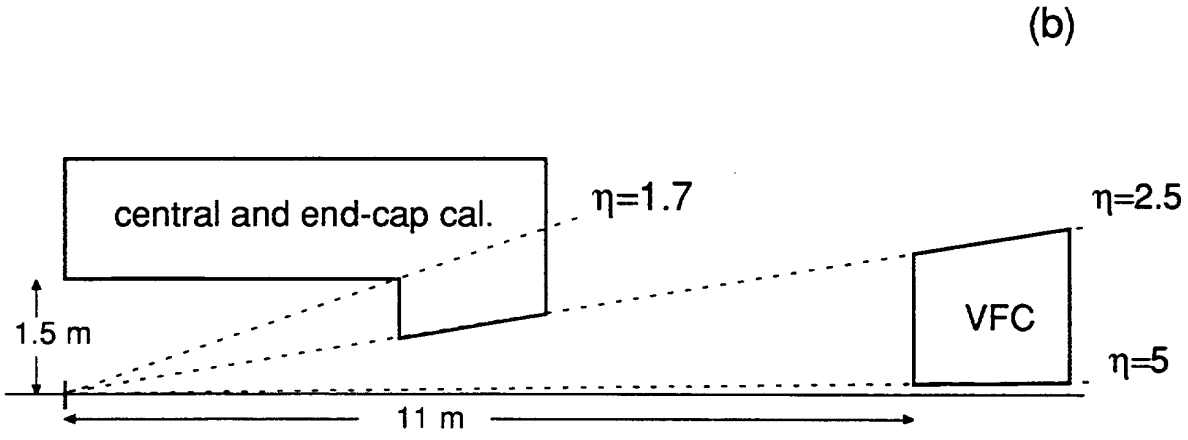
(b)
central and end-cap cal.
η=1.7
η=2.5
VFC
η=5
1.5 m
11 m

Figure 1

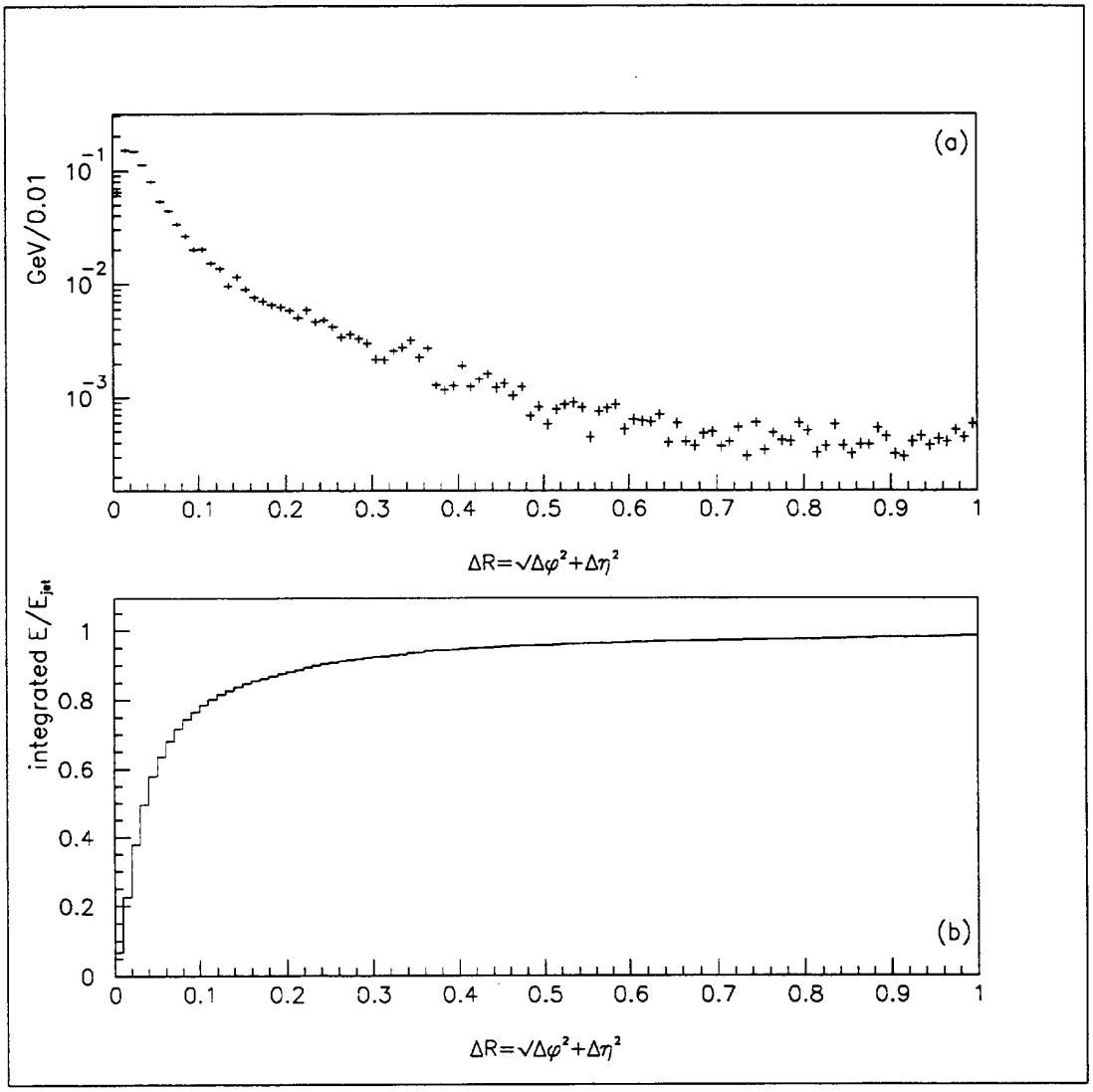
(a)
GeV/0.01
10^{-1}
10^{-2}
10^{-3}
0
0.1
0.2
0.3
0.4
0.5
0.6
0.7
0.8
0.9
1
$\Delta R=\sqrt{\Delta\varphi^2+\Delta\eta^2}$
integrated E/E_{jet}
1
0.8
0.6
0.4
0.2
0
(b)
$\Delta R=\sqrt{\Delta\varphi^2+\Delta\eta^2}$

Figure 2

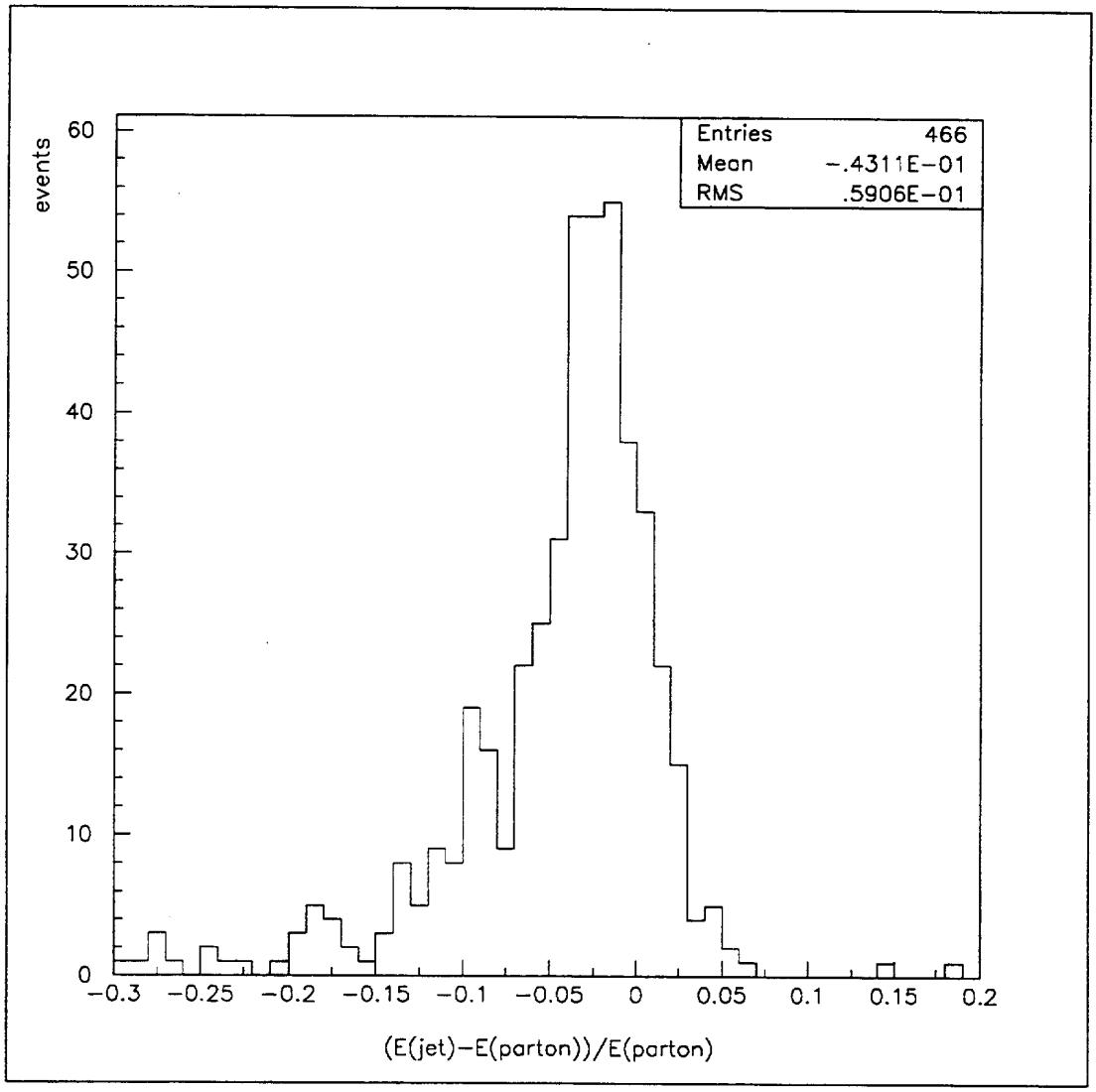
Entries 466
Mean −.4311E−01
RMS .5906E−01
events
60
50
40
30
20
10
0
−0.3 −0.25 −0.2 −0.15 −0.1 −0.05 0 0.05 0.1 0.15 0.2
(E(jet)−E(parton))/E(parton)

Figure 3

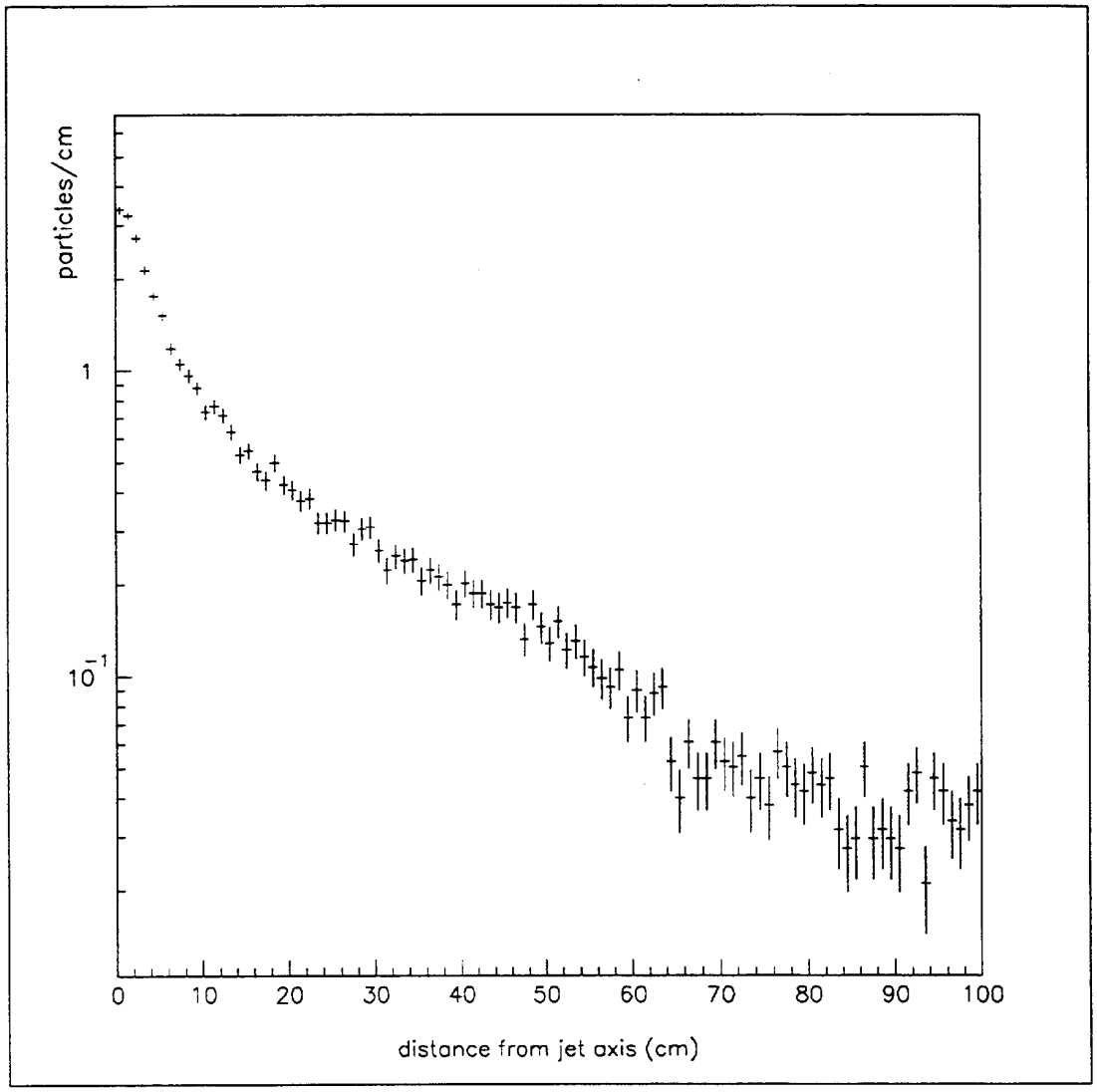
particles/cm
1
10^{-1}
0
10
20
30
40
50
60
70
80
90
100
distance from jet axis (cm)

Figure 4

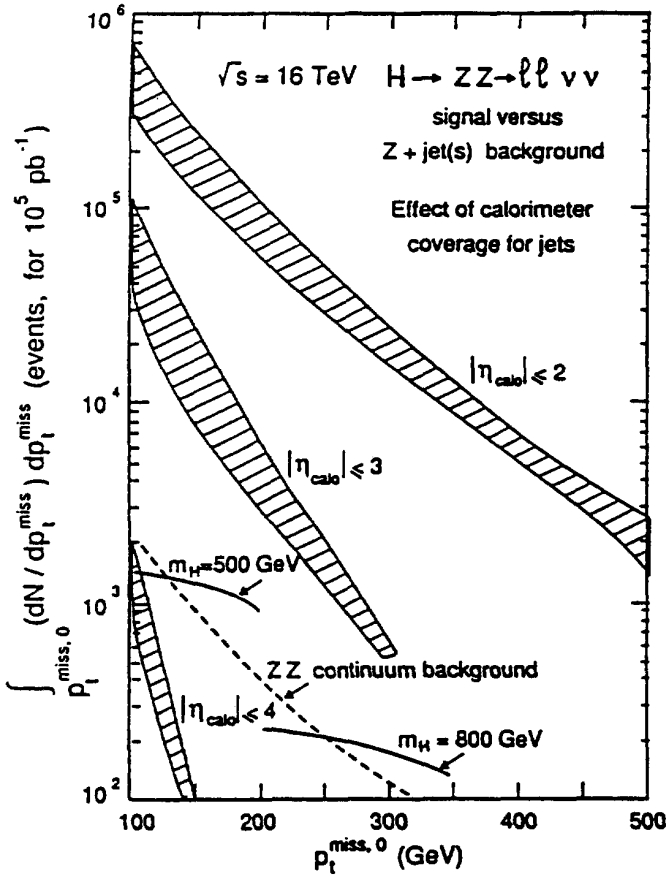

Figure 5

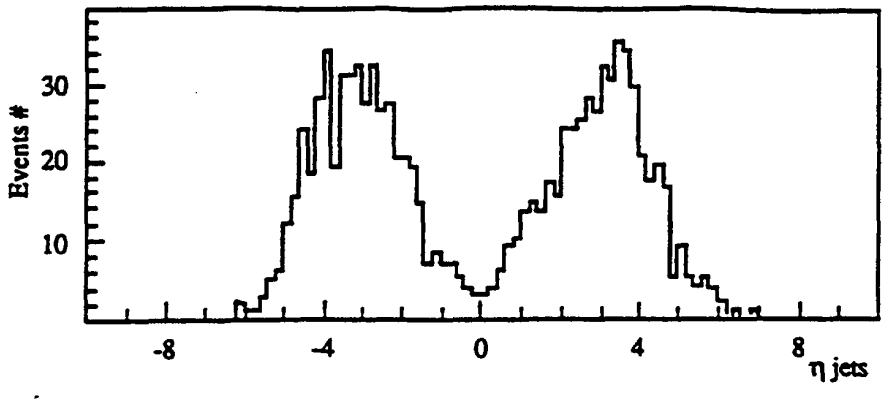

Figure 6

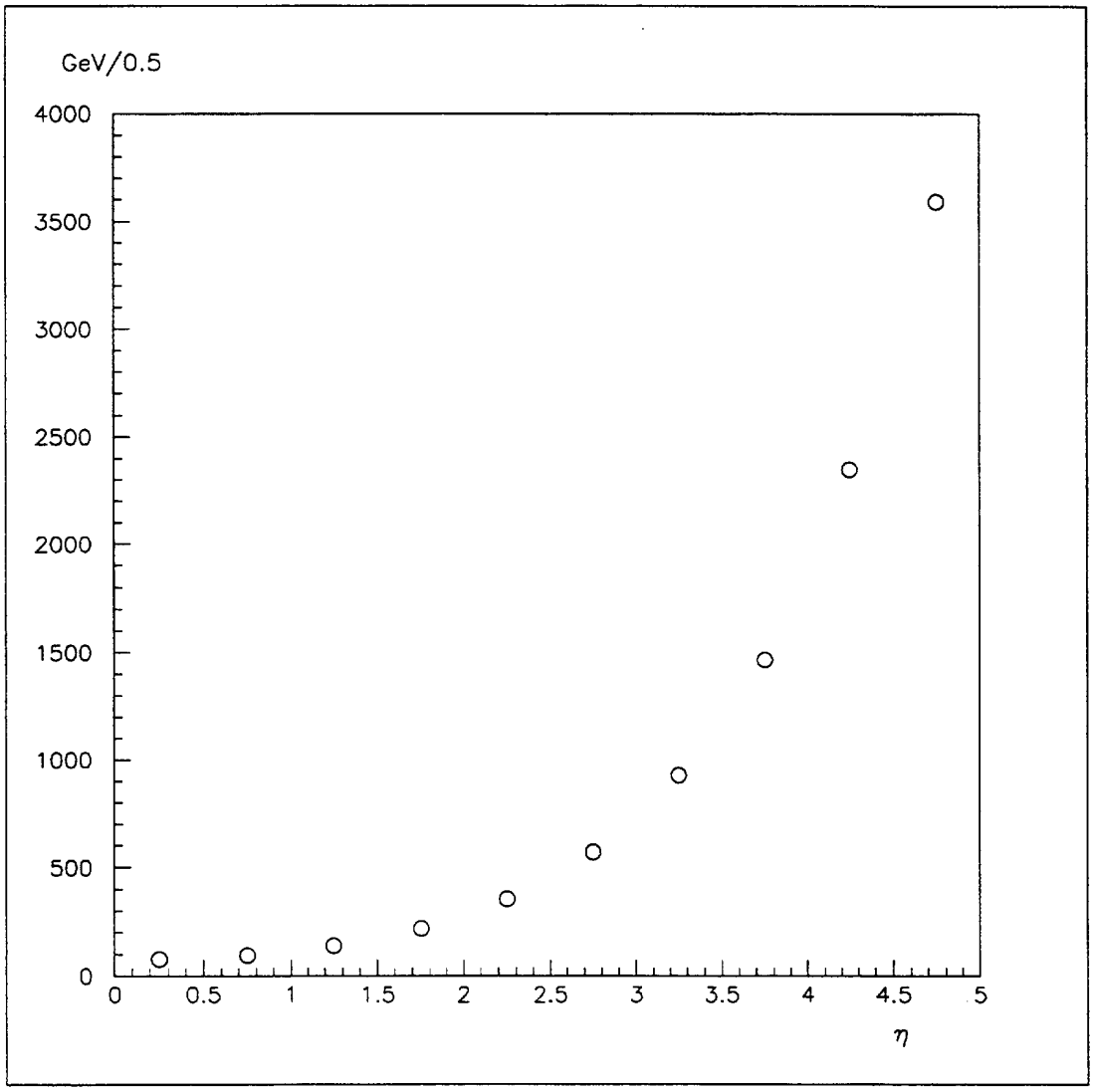
GeV/0.5
4000
3500
3000
2500
2000
1500
1000
500
0
0
0.5
1
1.5
2
2.5
3
3.5
4
4.5
5
η

Figure 7

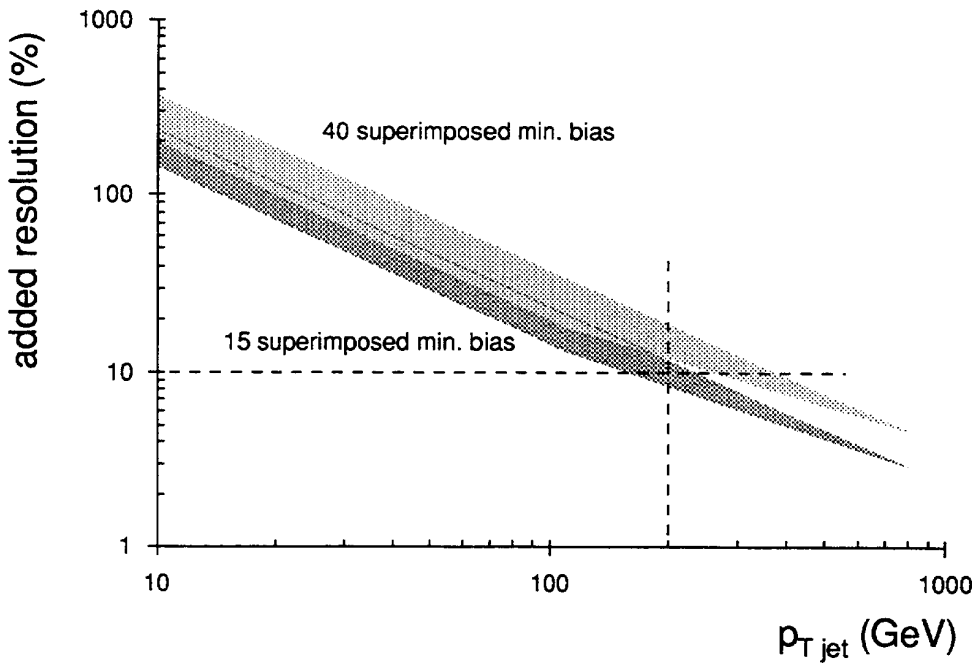
1000
100
10
1
added resolution (%)
40 superimposed min. bias
15 superimposed min. bias
10
100
1000
$p_{T\,jet}$ (GeV)

Figure 8

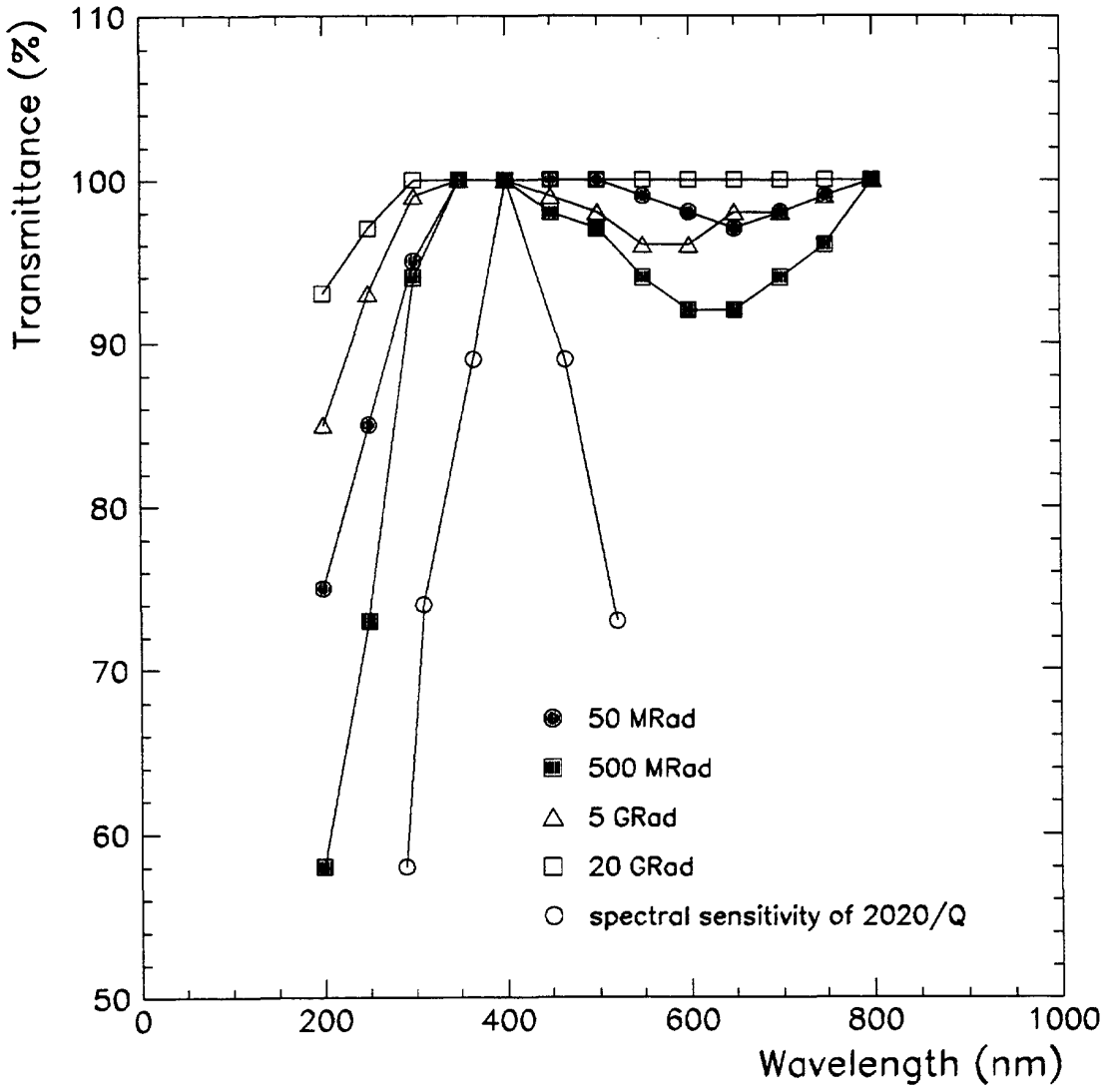
Transmittance (%)
110
100
90
80
70
60
50
0
200
400
600
800
1000
Wavelength (nm)
50 MRad
500 MRad
5 GRad
20 GRad
spectral sensitivity of 2020/Q

Figure 9

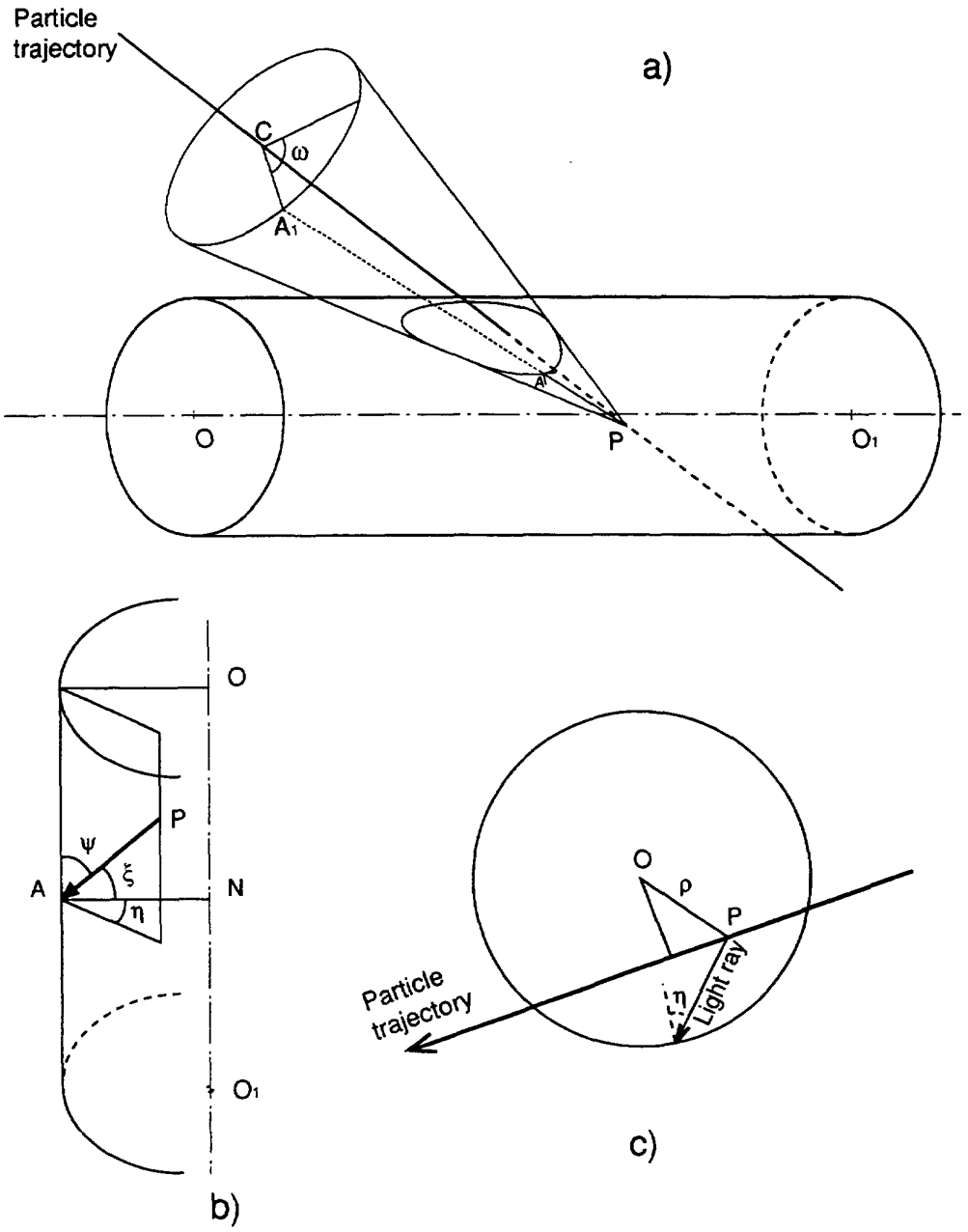
Particle
trajectory
a)
C
ω
A1
O
P
O1
O
P
ψ
ξ
A
N
η
O1
b)
O
ρ
P
Particle
trajectory
η
Light ray
c)

Figure 10

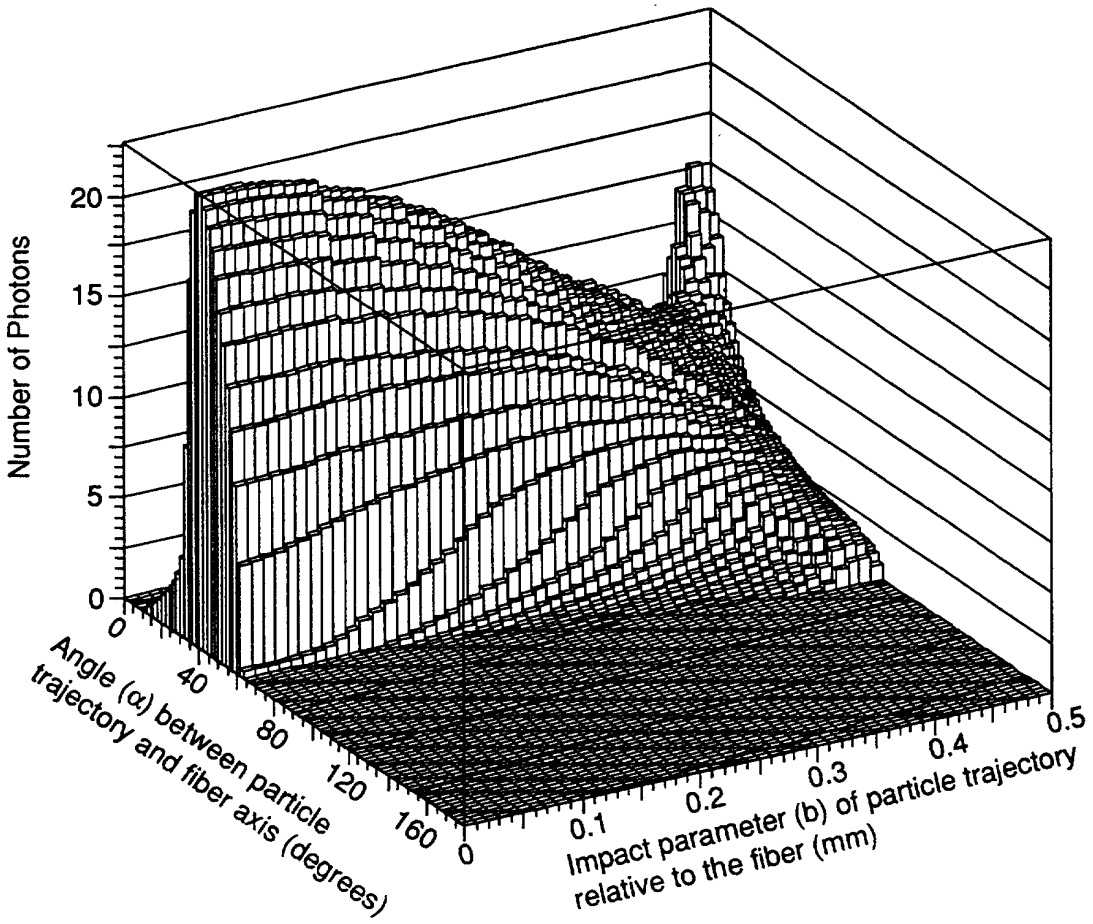
Number of Photons
20
15
10
5
0
0
40
80
120
160
Angle (α) between particle trajectory and fiber axis (degrees)
0
0.1
0.2
0.3
0.4
0.5
Impact parameter (b) of particle trajectory relative to the fiber (mm)

Figure 11

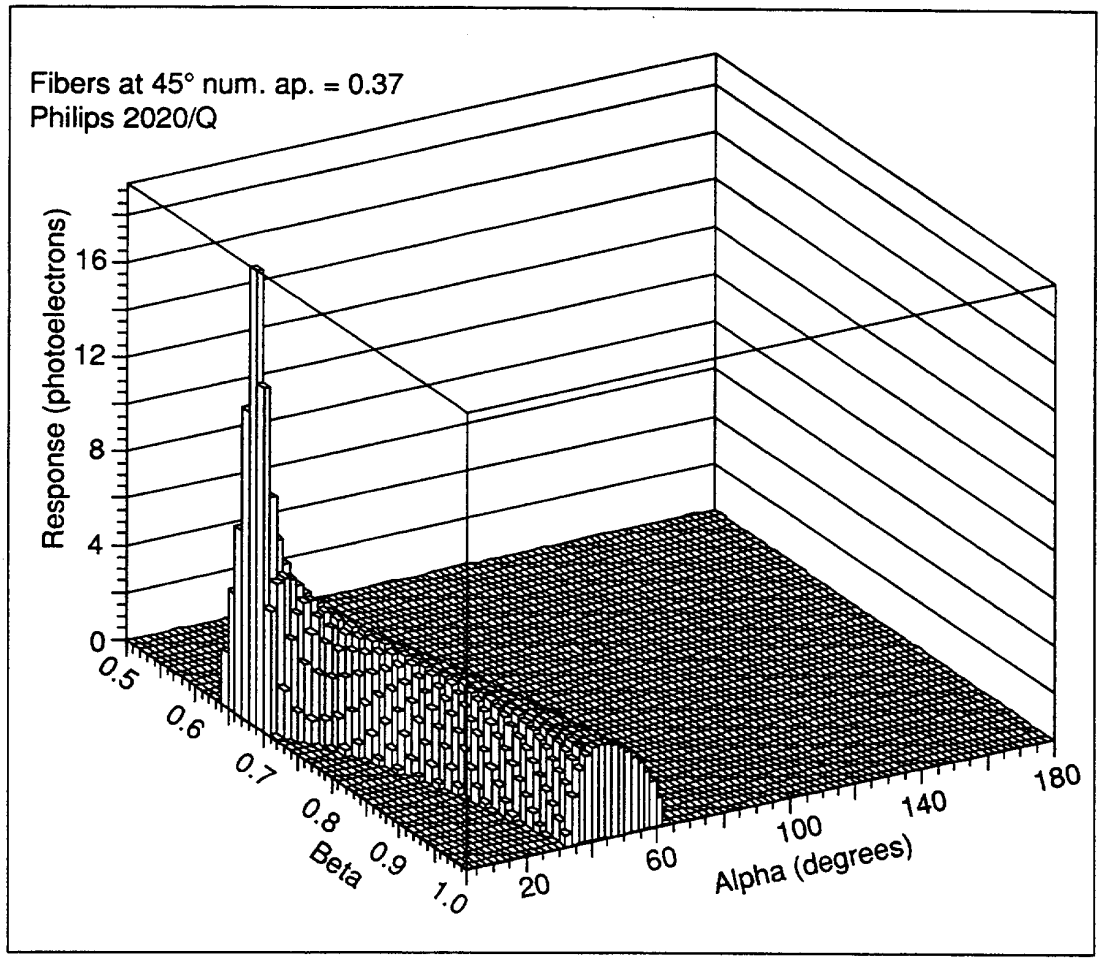
Fibers at 45° num. ap. = 0.37
Philips 2020/Q
Response (photoelectrons)
0
4
8
12
16
0.5
0.6
0.7
0.8
0.9
1.0
Beta
20
60
100
140
180
Alpha (degrees)

Figure 12

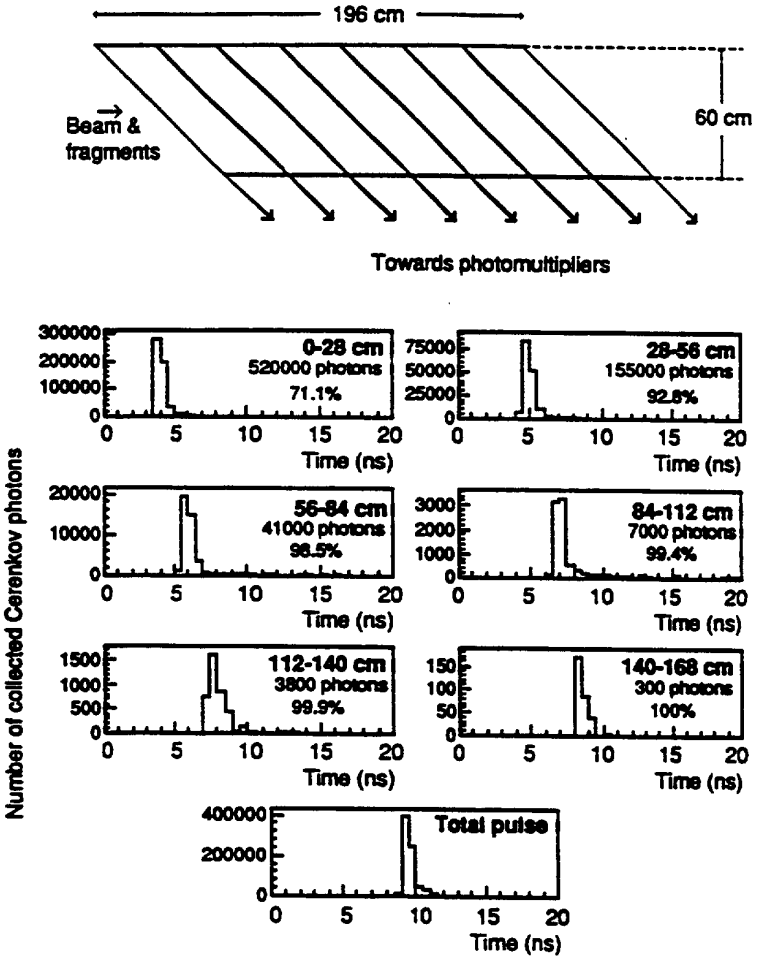
196 cm
60 cm
Beam &
fragments
Towards photomultipliers
Number of collected Cerenkov photons
0-28 cm
520000 photons
71.1%
28-56 cm
155000 photons
92.8%
56-84 cm
41000 photons
98.5%
84-112 cm
7000 photons
99.4%
112-140 cm
3800 photons
99.9%
140-168 cm
300 photons
100%
Total pulse
Time (ns)

Figure 13

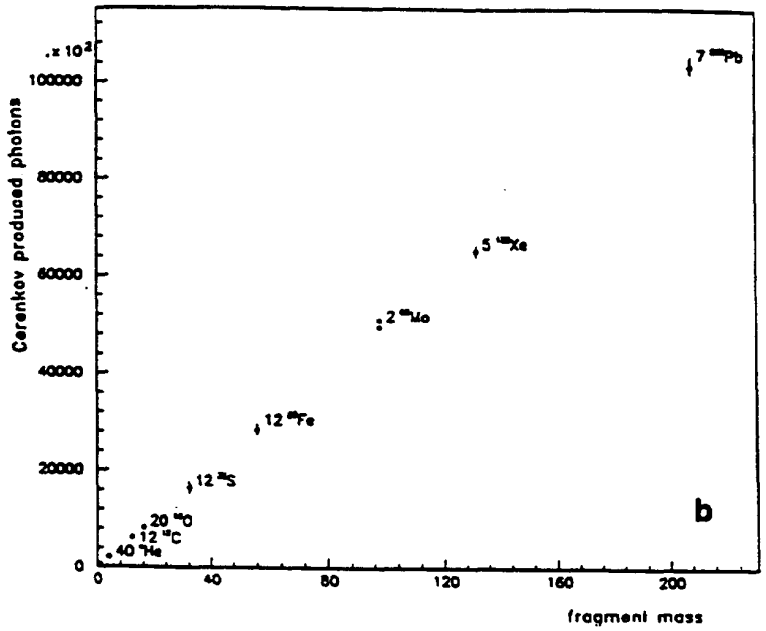

Figure 14

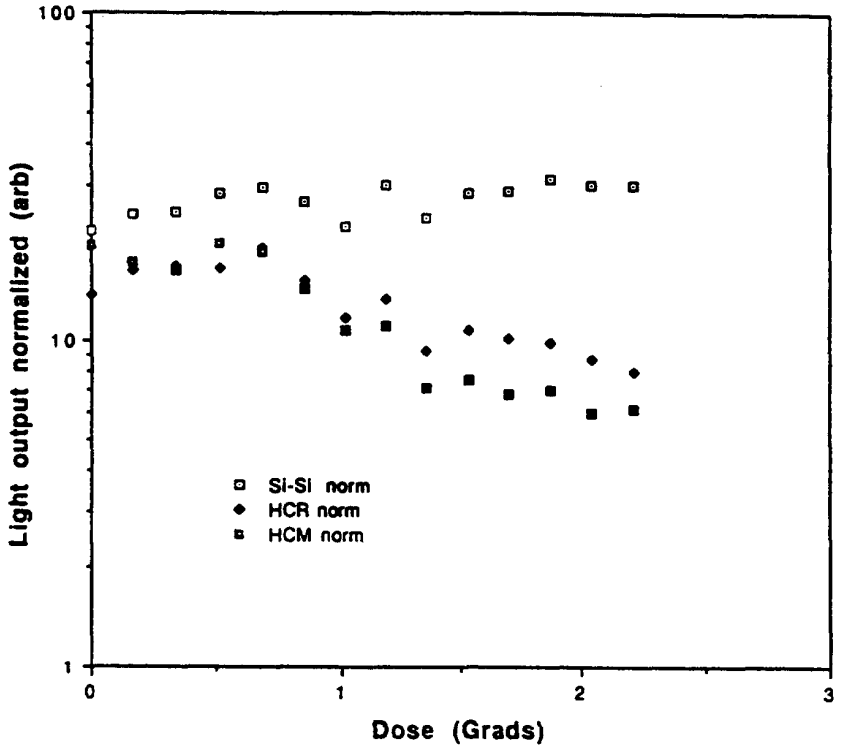

Figure 15

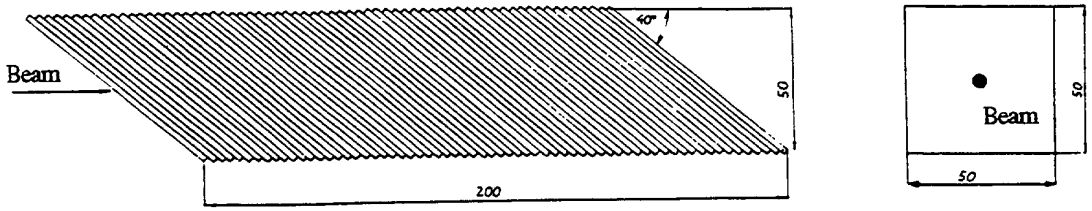

Figure 16

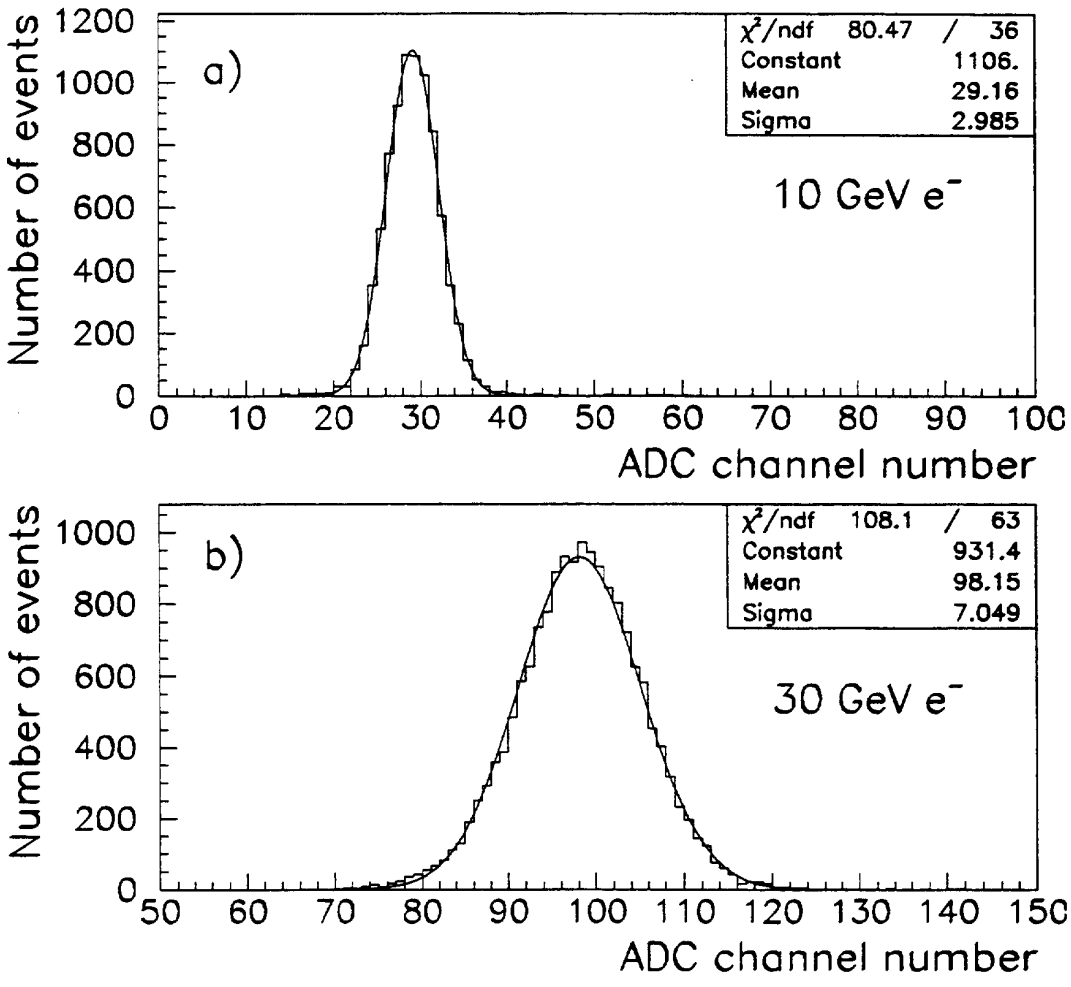

Figure 17

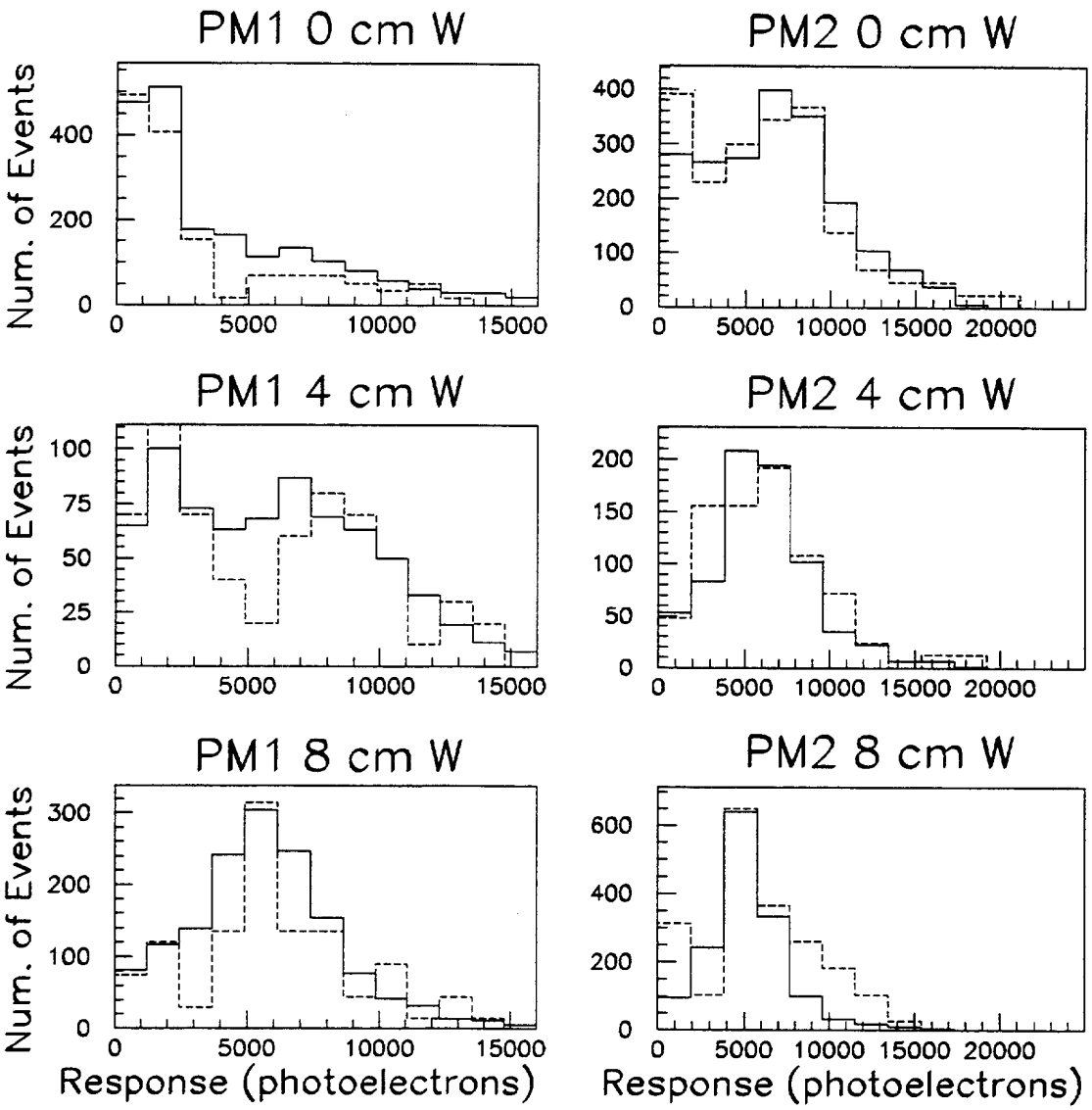
PM1 0 cm W
PM2 0 cm W
PM1 4 cm W
PM2 4 cm W
PM1 8 cm W
PM2 8 cm W
Num. of Events
Response (photoelectrons)
0
5000
10000
15000
20000

Figure 18

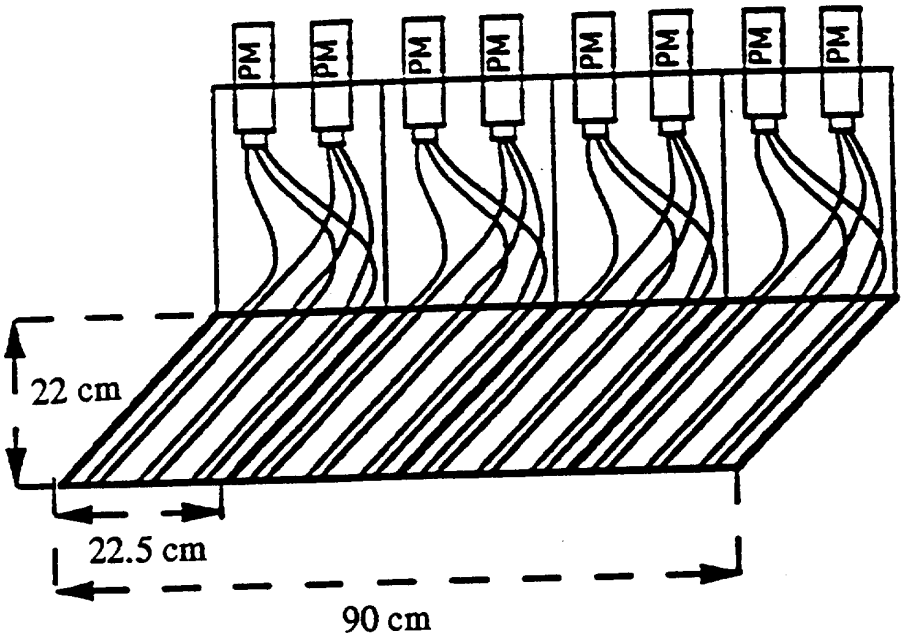

Figure 19

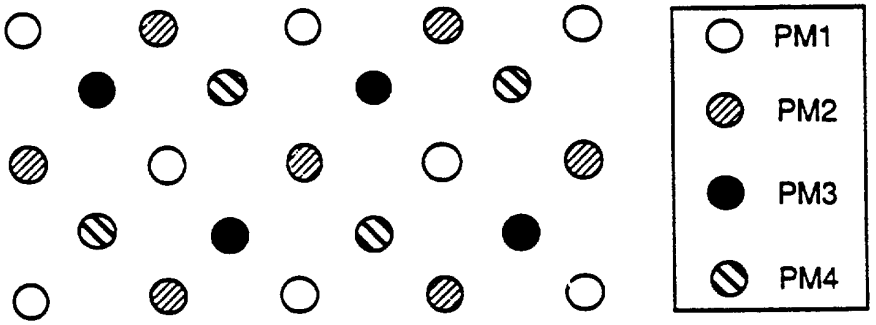

Figure 20

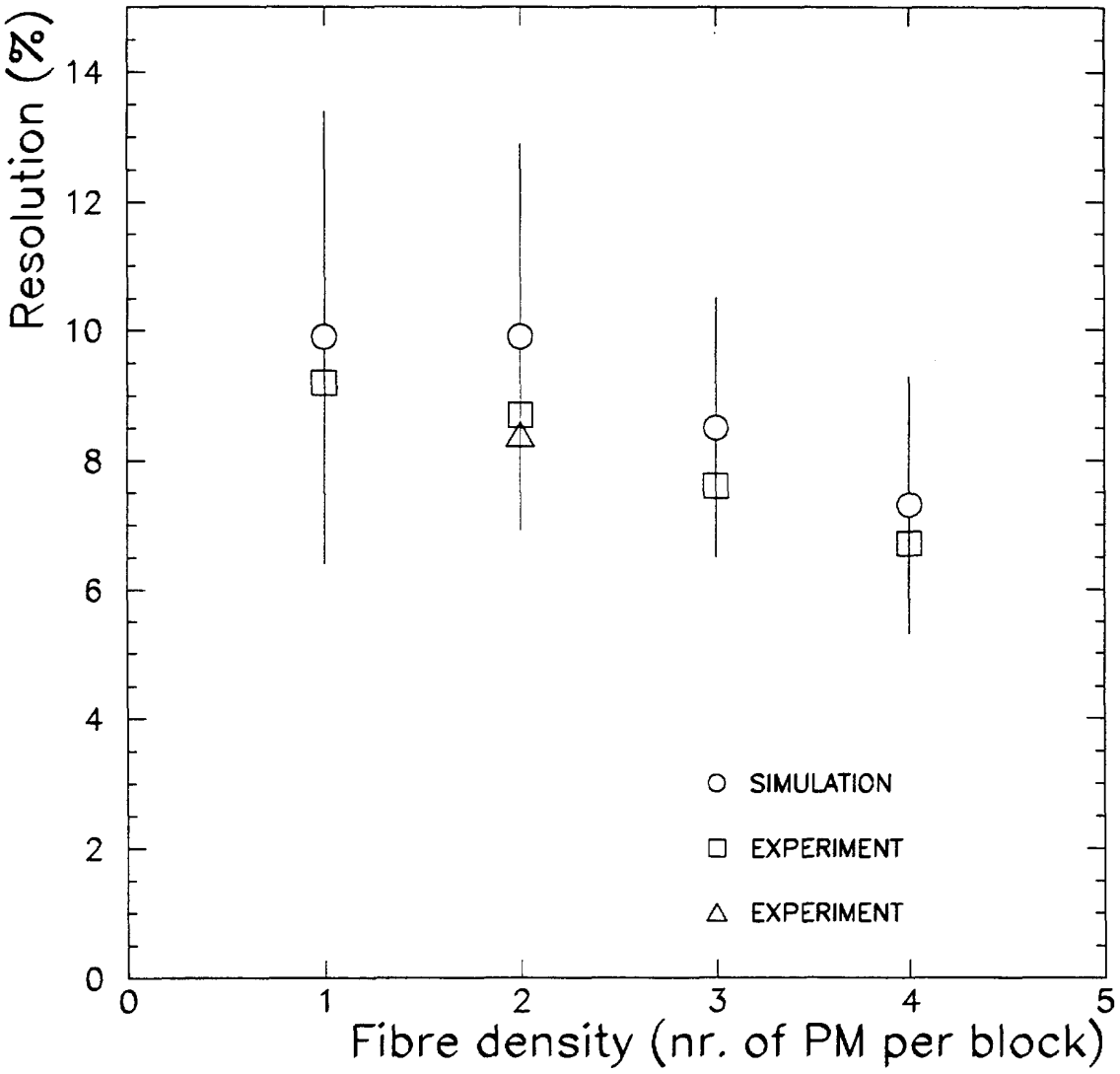
Resolution (%)
14
12
10
8
6
4
2
0
0
1
2
3
4
5
Fibre density (nr. of PM per block)
SIMULATION
EXPERIMENT
EXPERIMENT

Figure 21

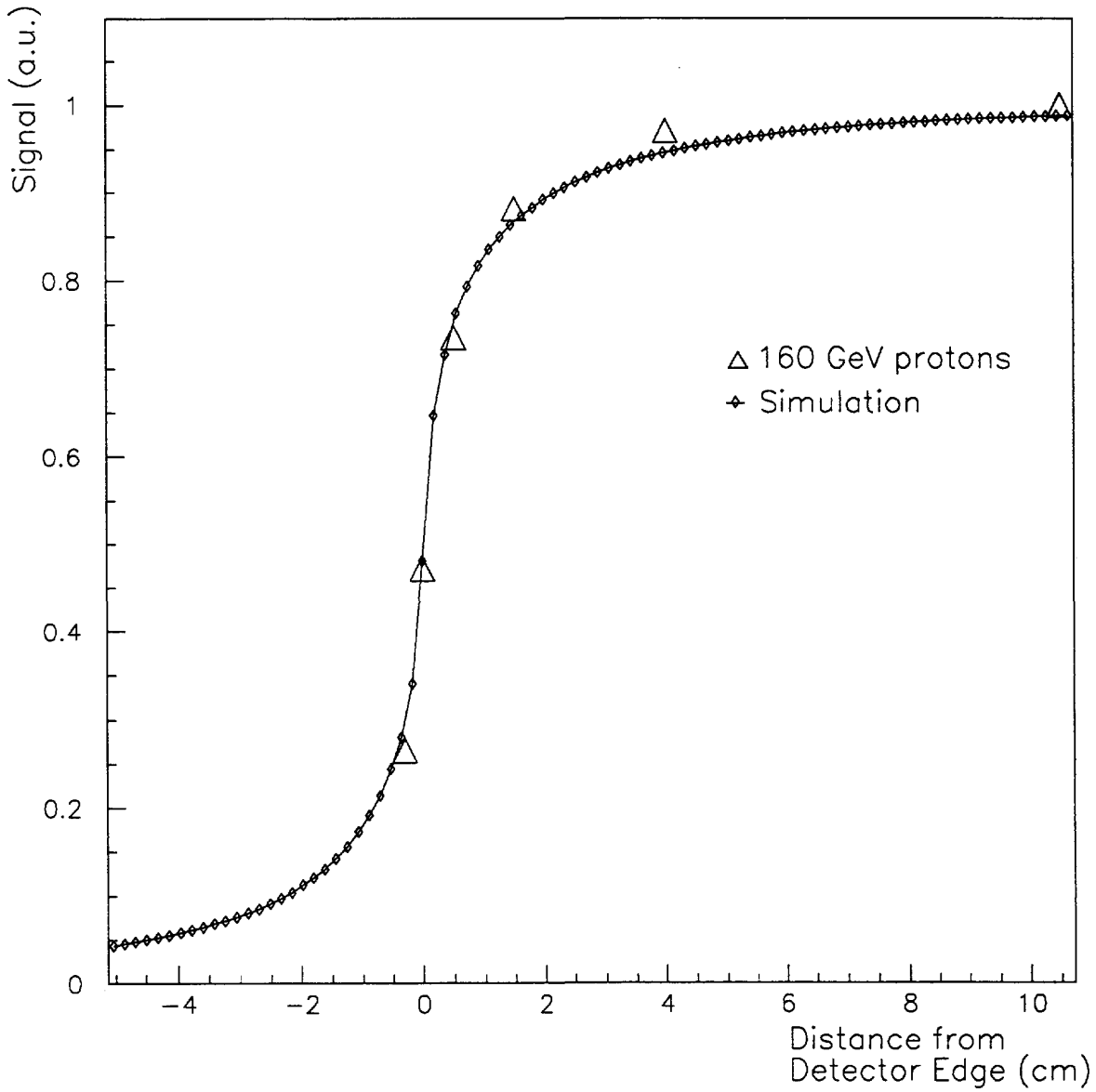
Signal (a.u.)
1
0.8
0.6
0.4
0.2
0
−4
−2
0
2
4
6
8
10
Distance from
Detector Edge (cm)
△ 160 GeV protons
Simulation

Figure 22

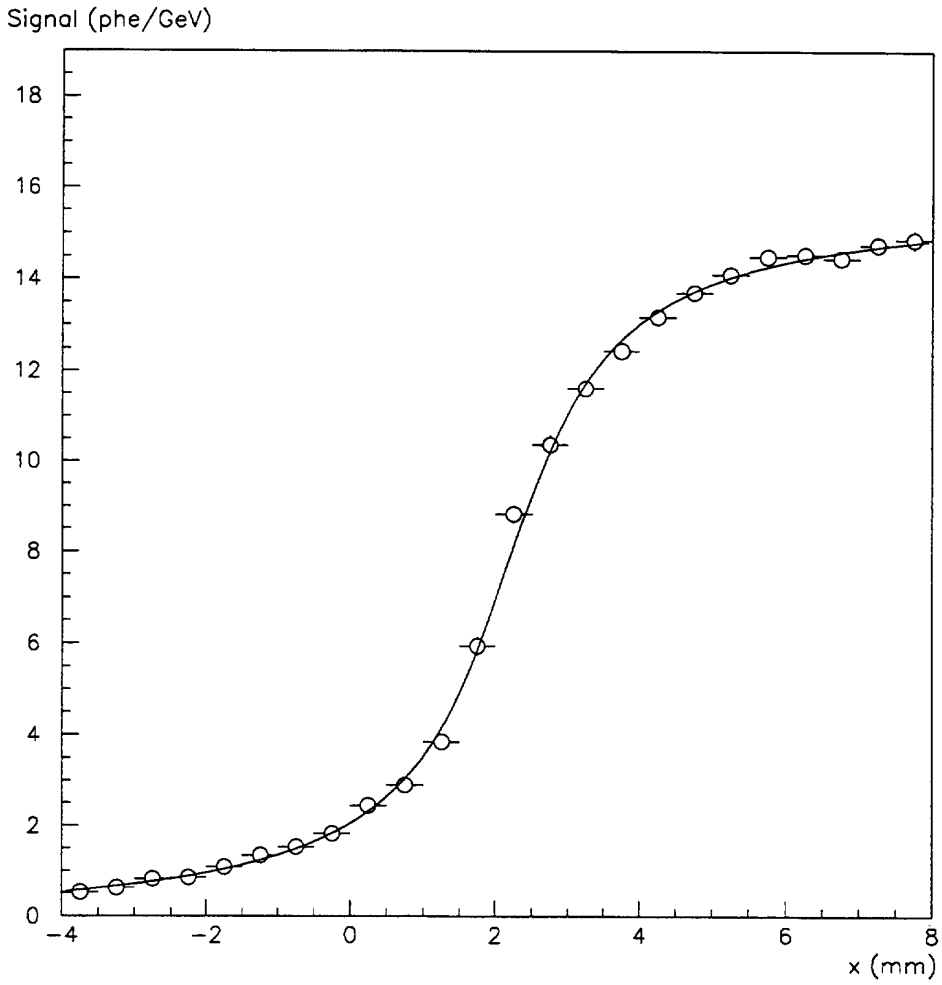

Figure 23

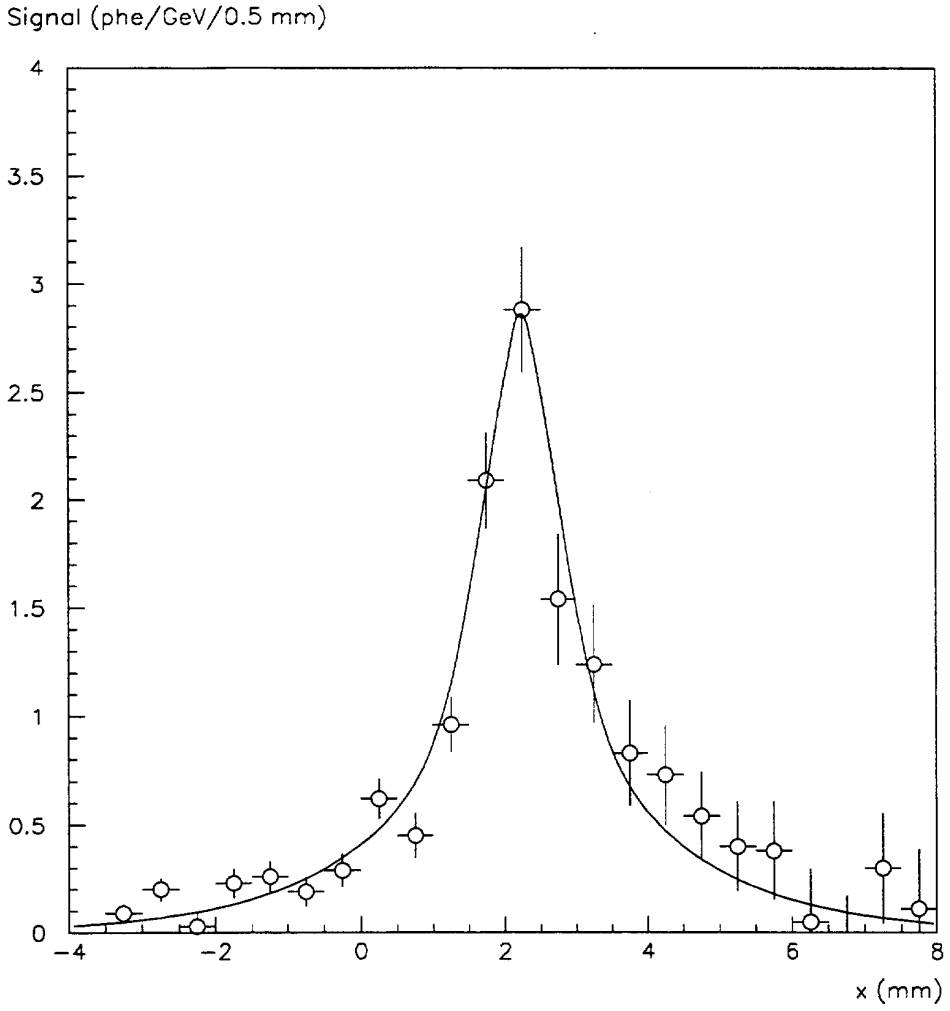

Figure 24

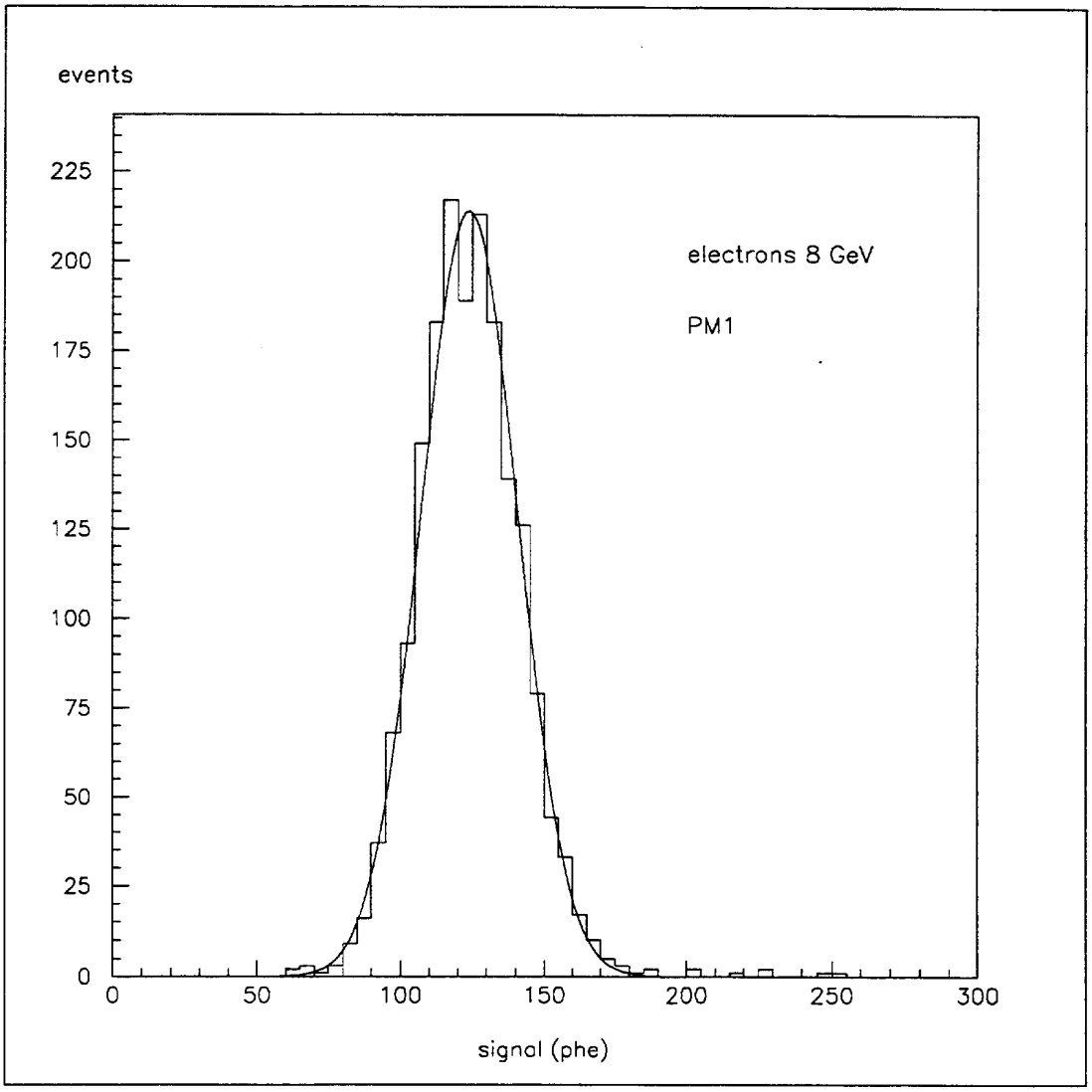
events
225
200
175
150
125
100
75
50
25
0
0
50
100
150
200
250
300
signal (phe)
electrons 8 GeV
PM1

Figure 25

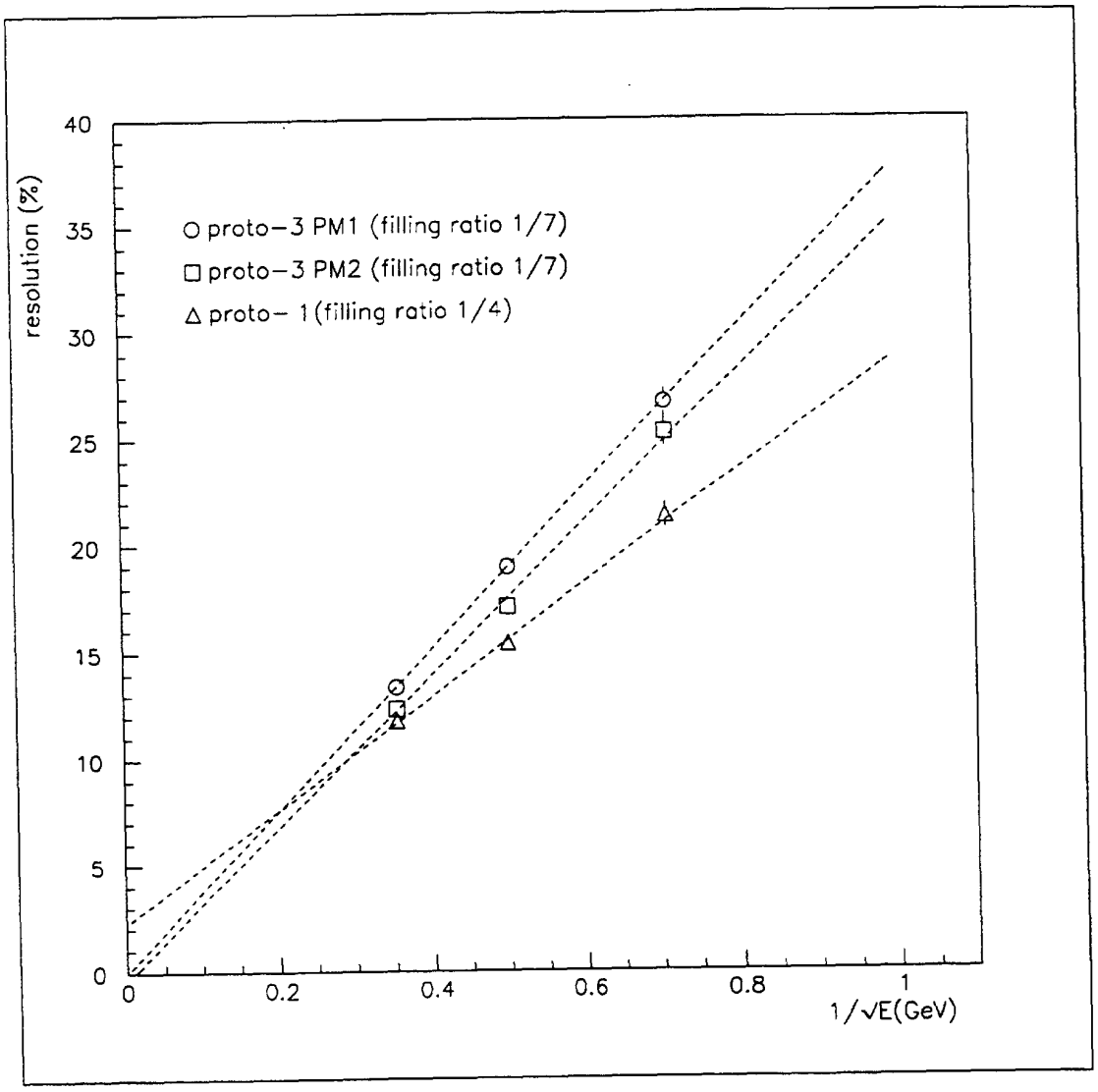
resolution (%)
40
35
30
25
20
15
10
5
0
0
0.2
0.4
0.6
0.8
1
1/√E(GeV)
○ proto−3 PM1 (filling ratio 1/7)
□ proto−3 PM2 (filling ratio 1/7)
△ proto− 1 (filling ratio 1/4)

Figure 26

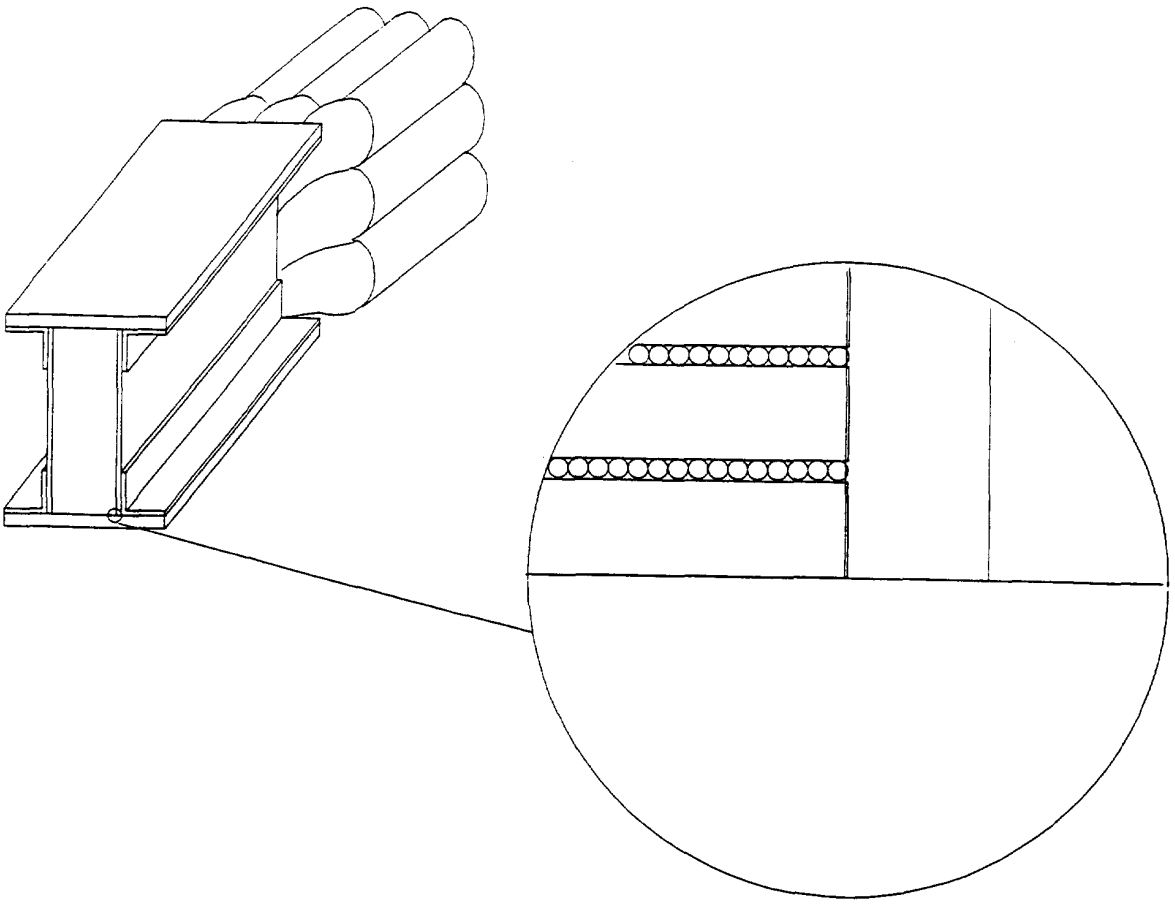

Figure 27

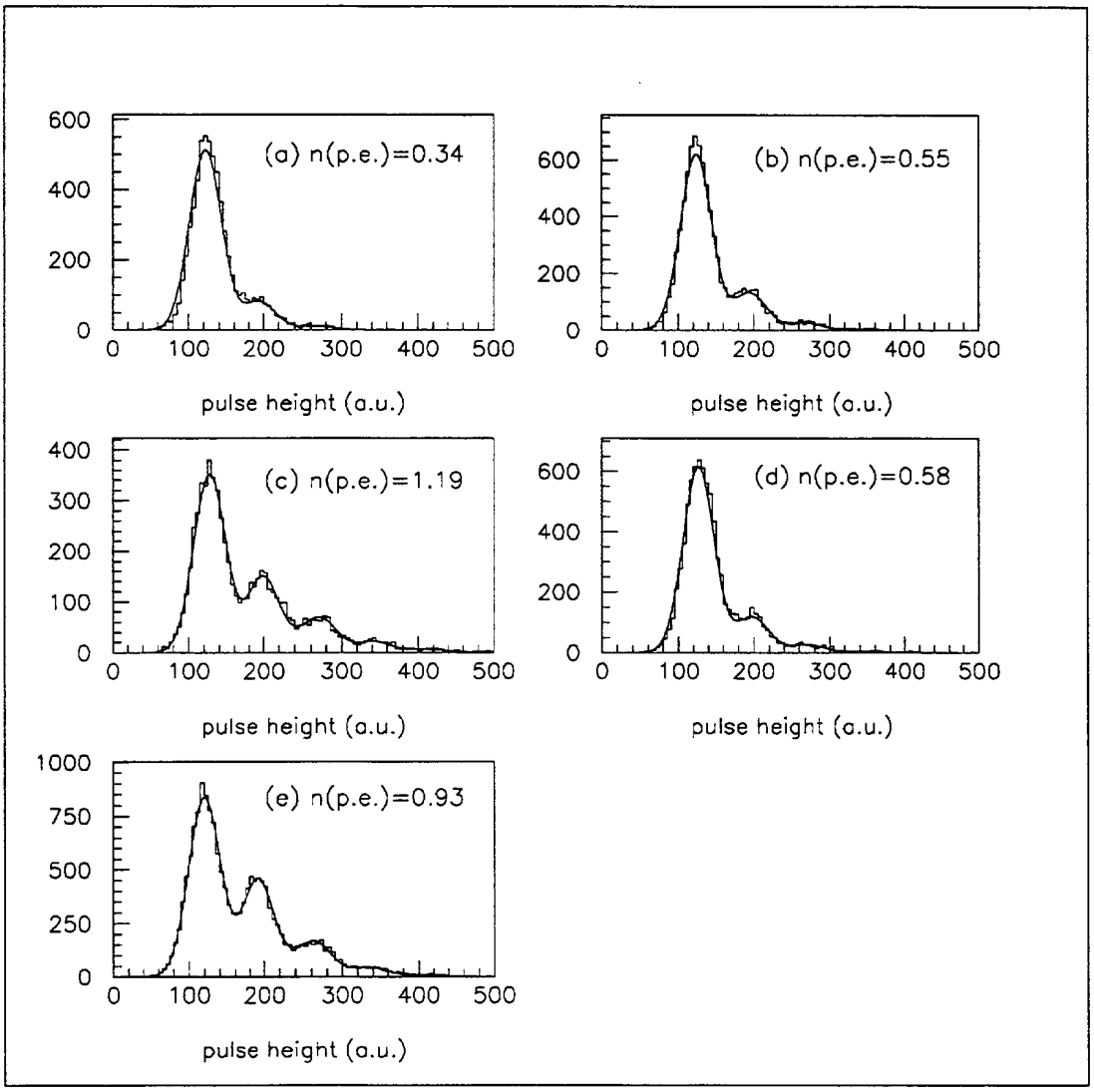

Figure 28

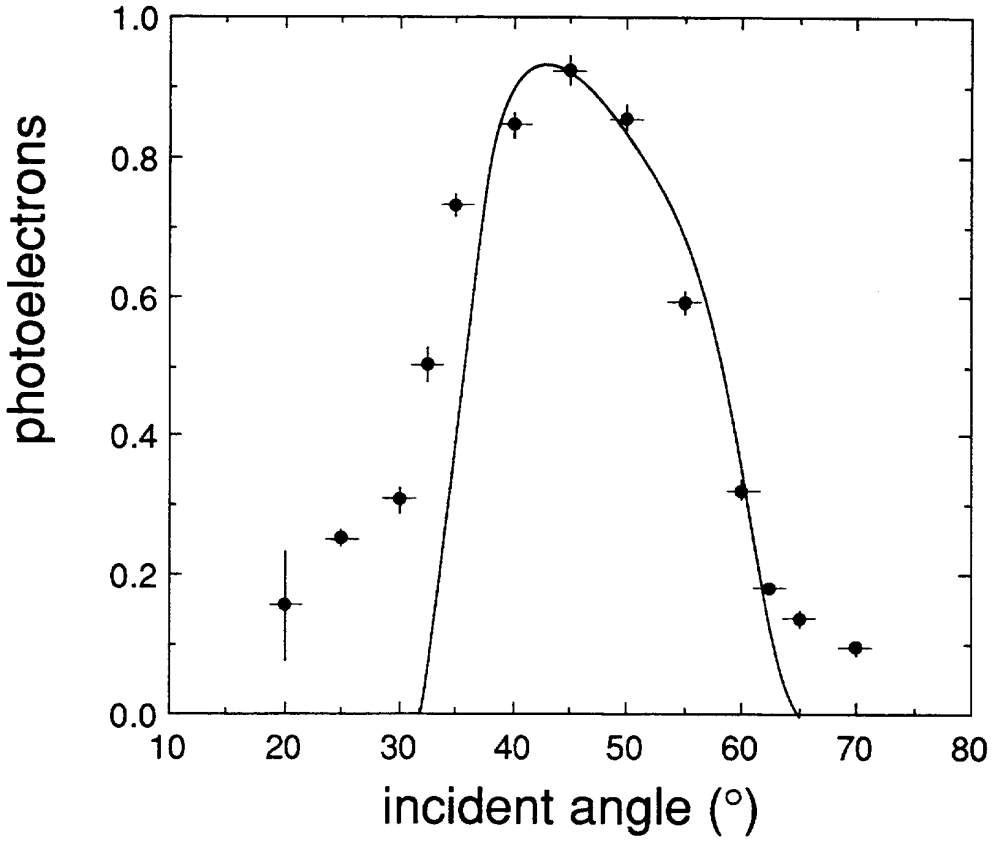
photoelectrons
1.0
0.8
0.6
0.4
0.2
0.0
10
20
30
40
50
60
70
80
incident angle (°)

Figure 29

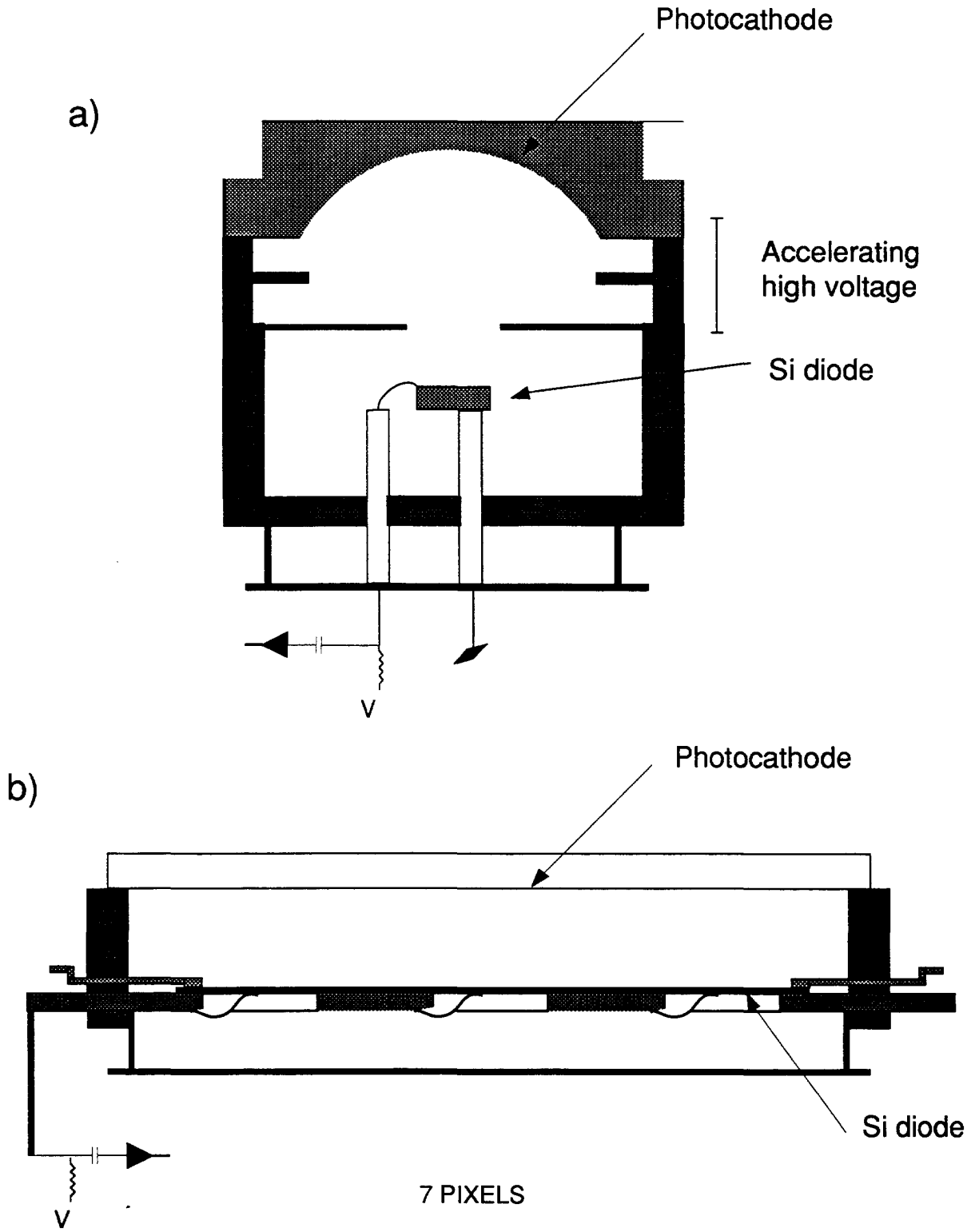
a)
Photocathode
Accelerating
high voltage
Si diode
V
b)
Photocathode
Si diode
V
7 PIXELS

Figure 30

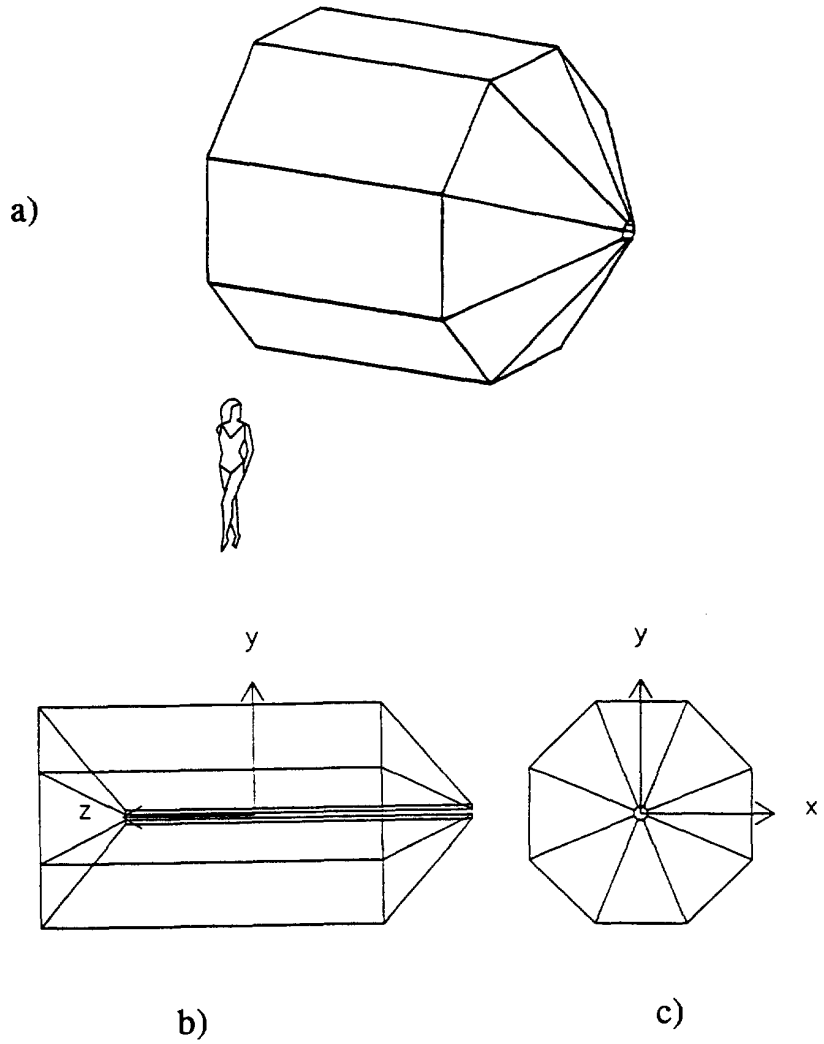

Figure 31

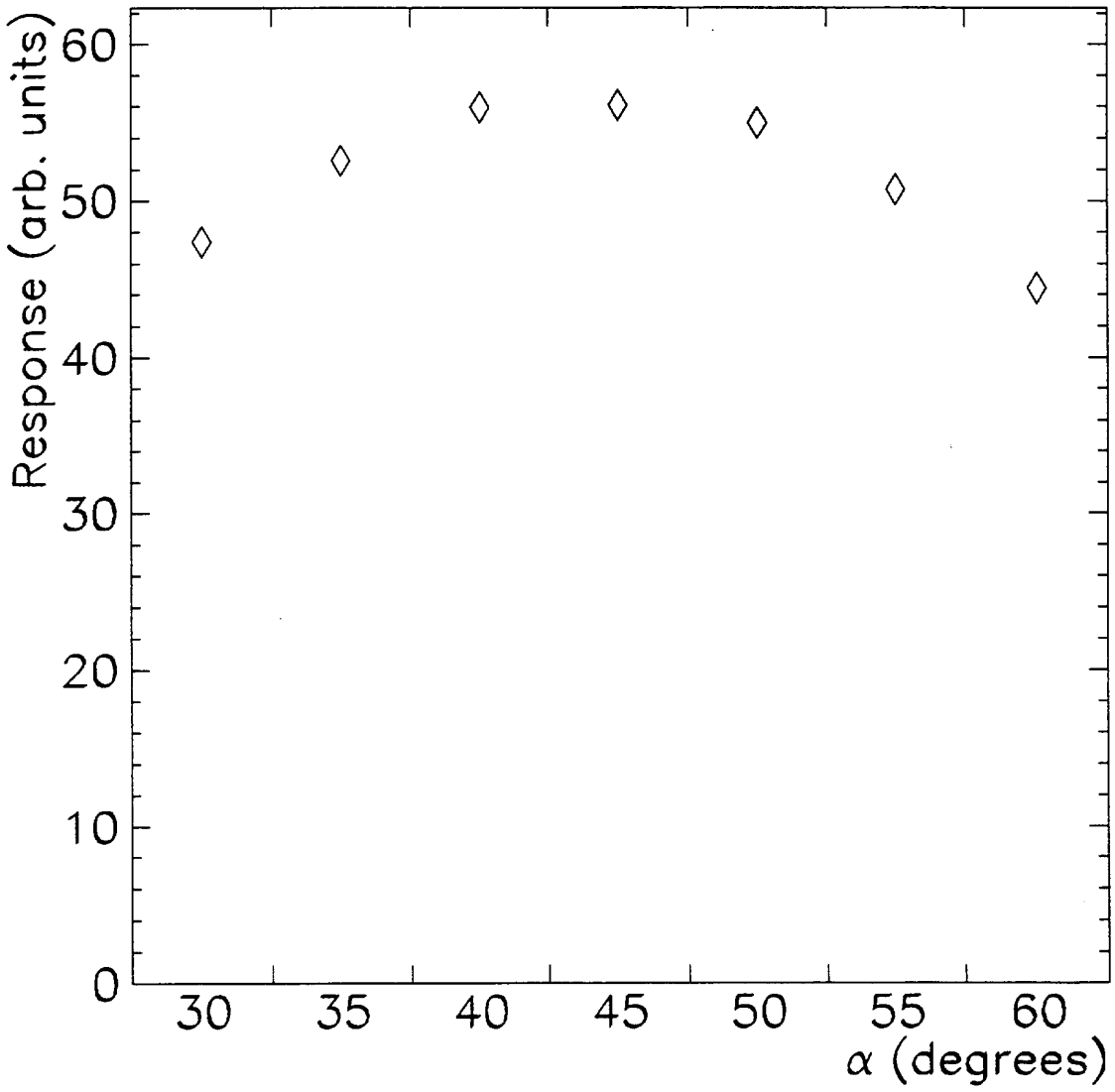
Response (arb. units)
0
10
20
30
40
50
60
30
35
40
45
50
55
60
α (degrees)

Figure 32

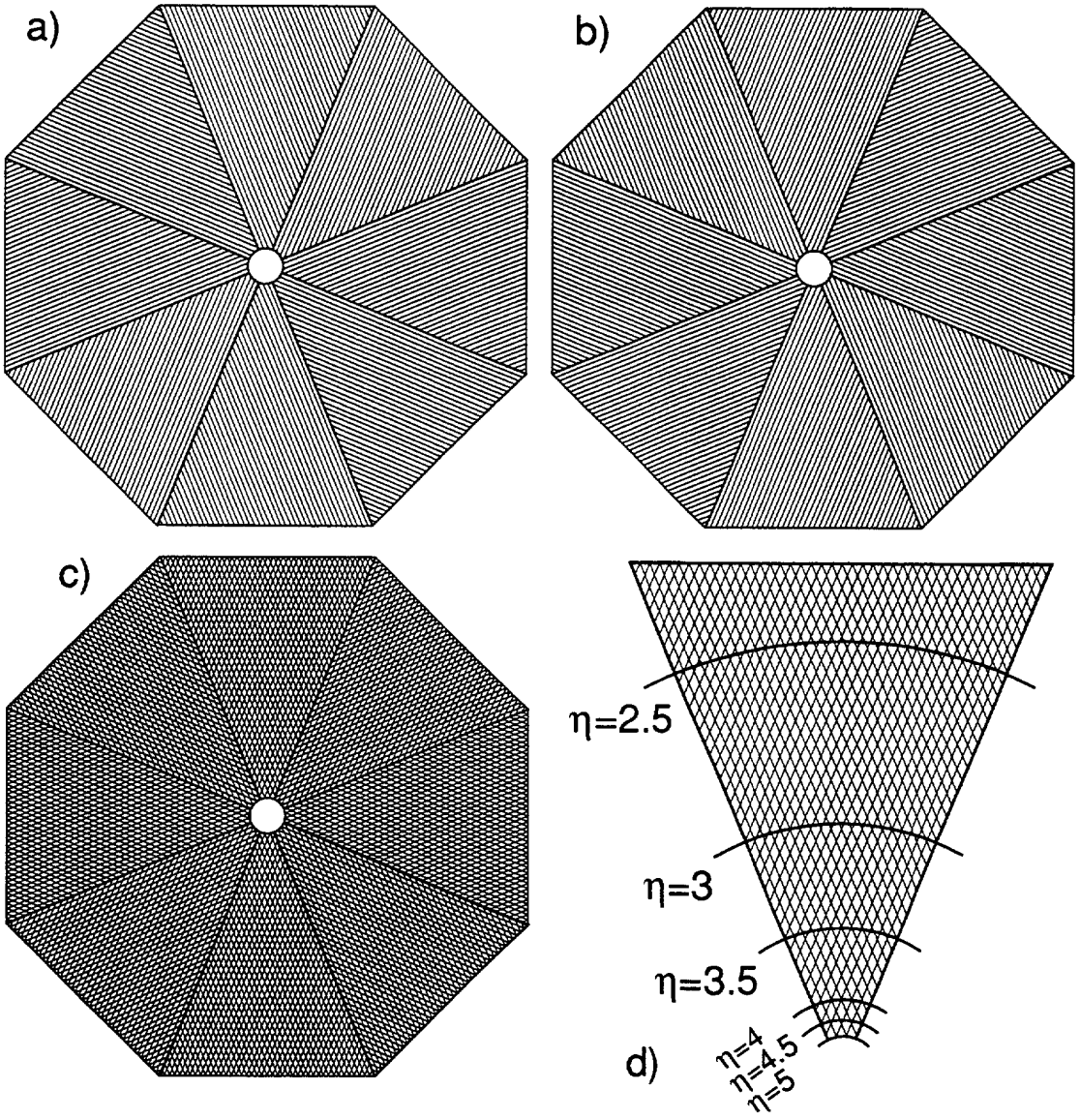

Figure 33

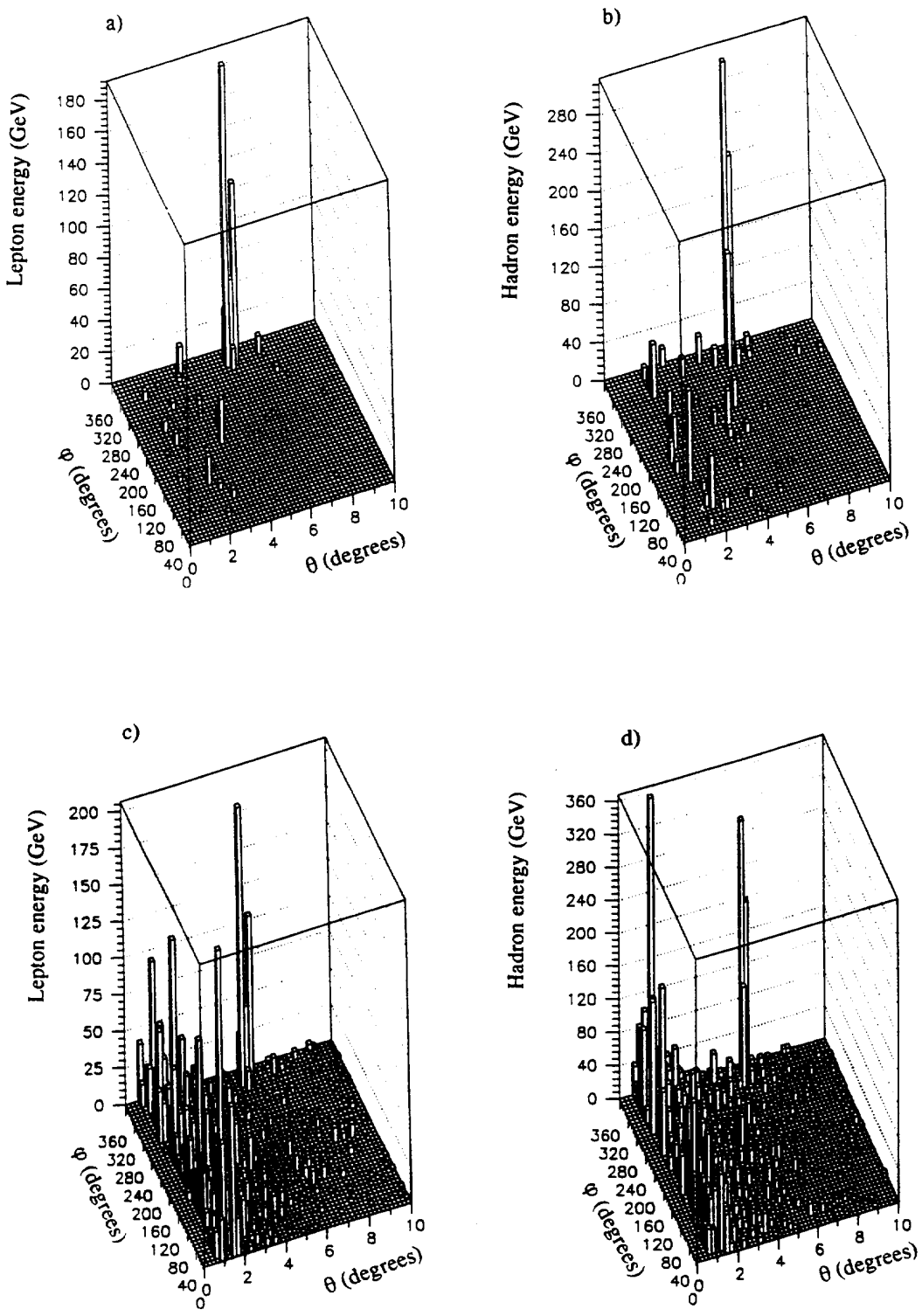
a)
Lepton energy (GeV)
180
160
140
120
100
80
60
40
20
0
360
320
280
240
200
160
120
80
40
0
φ (degrees)
0
2
4
6
8
10
θ (degrees)
b)
Hadron energy (GeV)
280
240
200
160
120
80
40
0
360
320
280
240
200
160
120
80
40
0
φ (degrees)
0
2
4
6
8
10
θ (degrees)
c)
Lepton energy (GeV)
200
175
150
125
100
75
50
25
0
360
320
280
240
200
160
120
80
40
0
φ (degrees)
0
2
4
6
8
10
θ (degrees)
d)
Hadron energy (GeV)
360
320
280
240
200
160
120
80
40
0
360
320
280
240
200
160
120
80
40
0
φ (degrees)
0
2
4
6
8
10
θ (degrees)

Figure 34

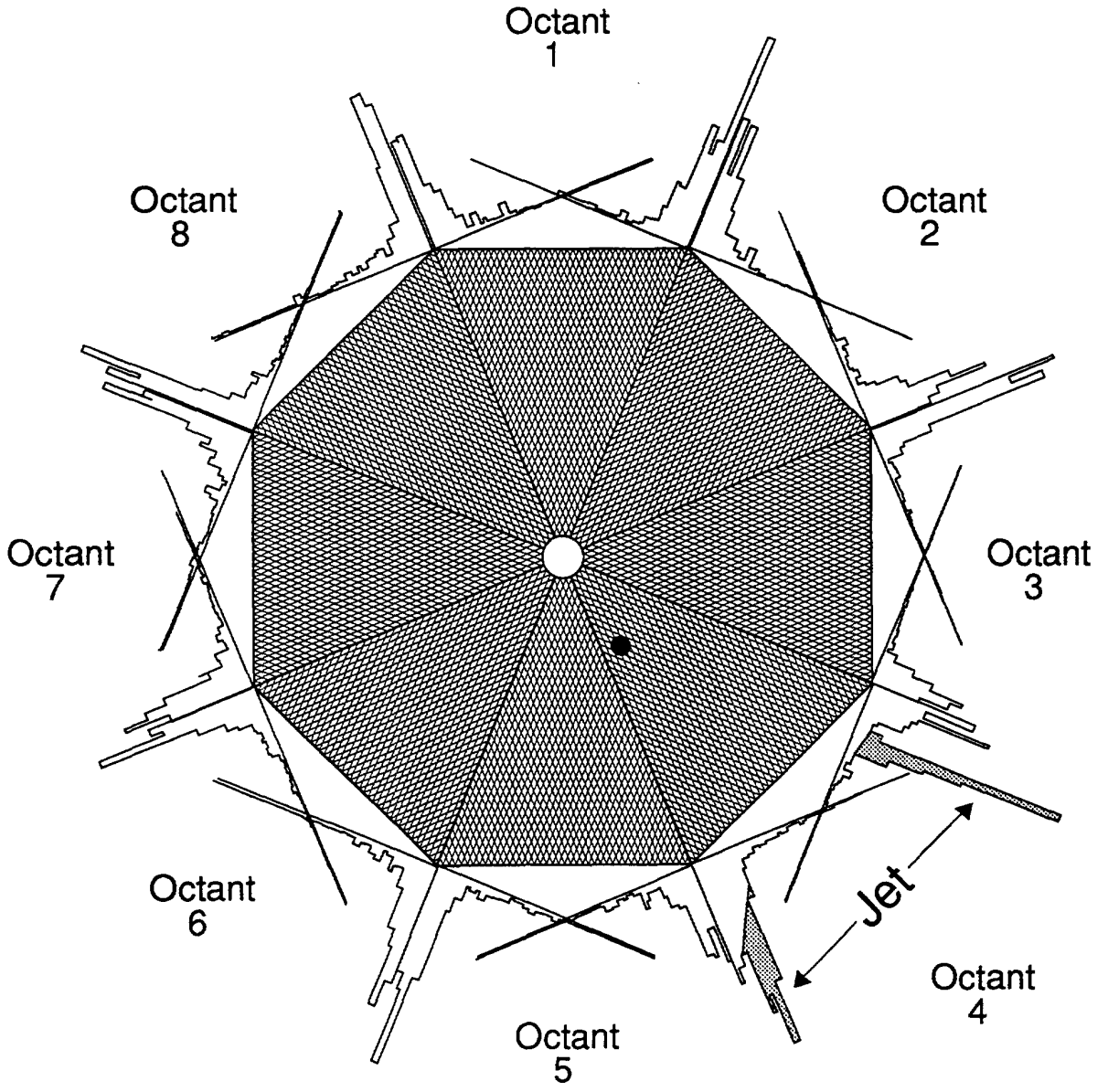
Octant
1
Octant
2
Octant
3
Octant
4
Octant
5
Octant
6
Octant
7
Octant
8
Jet

Figure 35

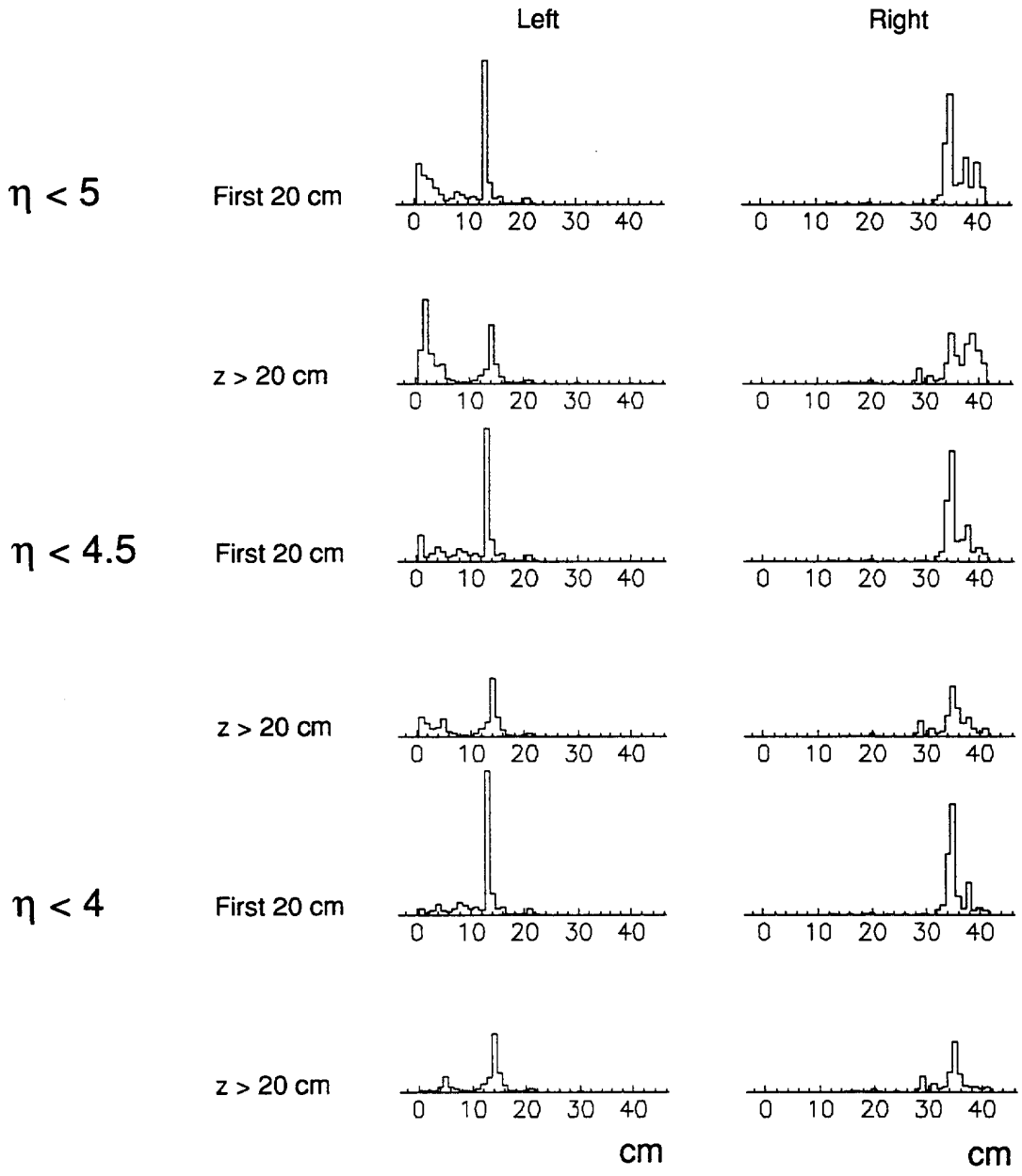
Left
Right
η < 5
First 20 cm
z > 20 cm
η < 4.5
First 20 cm
z > 20 cm
η < 4
First 20 cm
z > 20 cm
0 10 20 30 40
cm

Figure 36

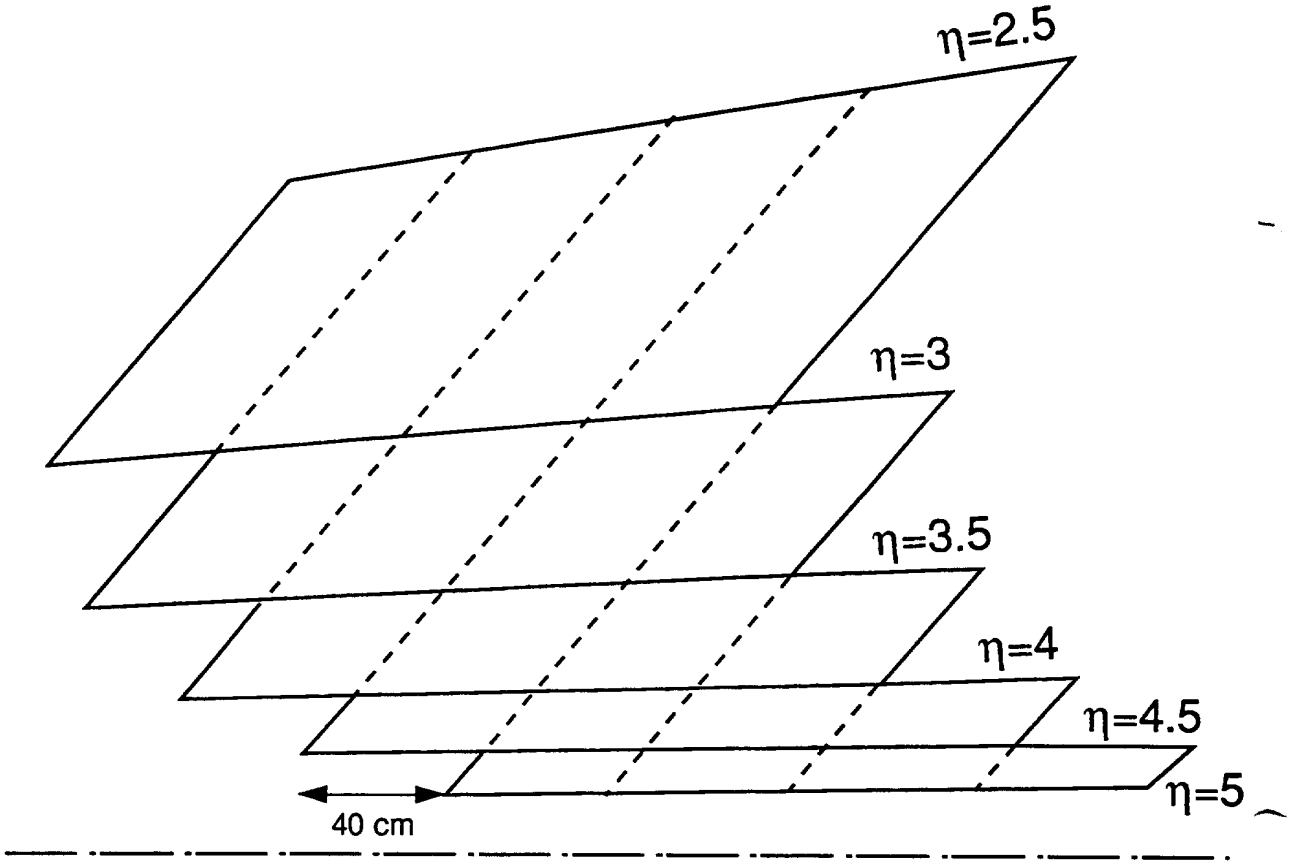

Figure 37

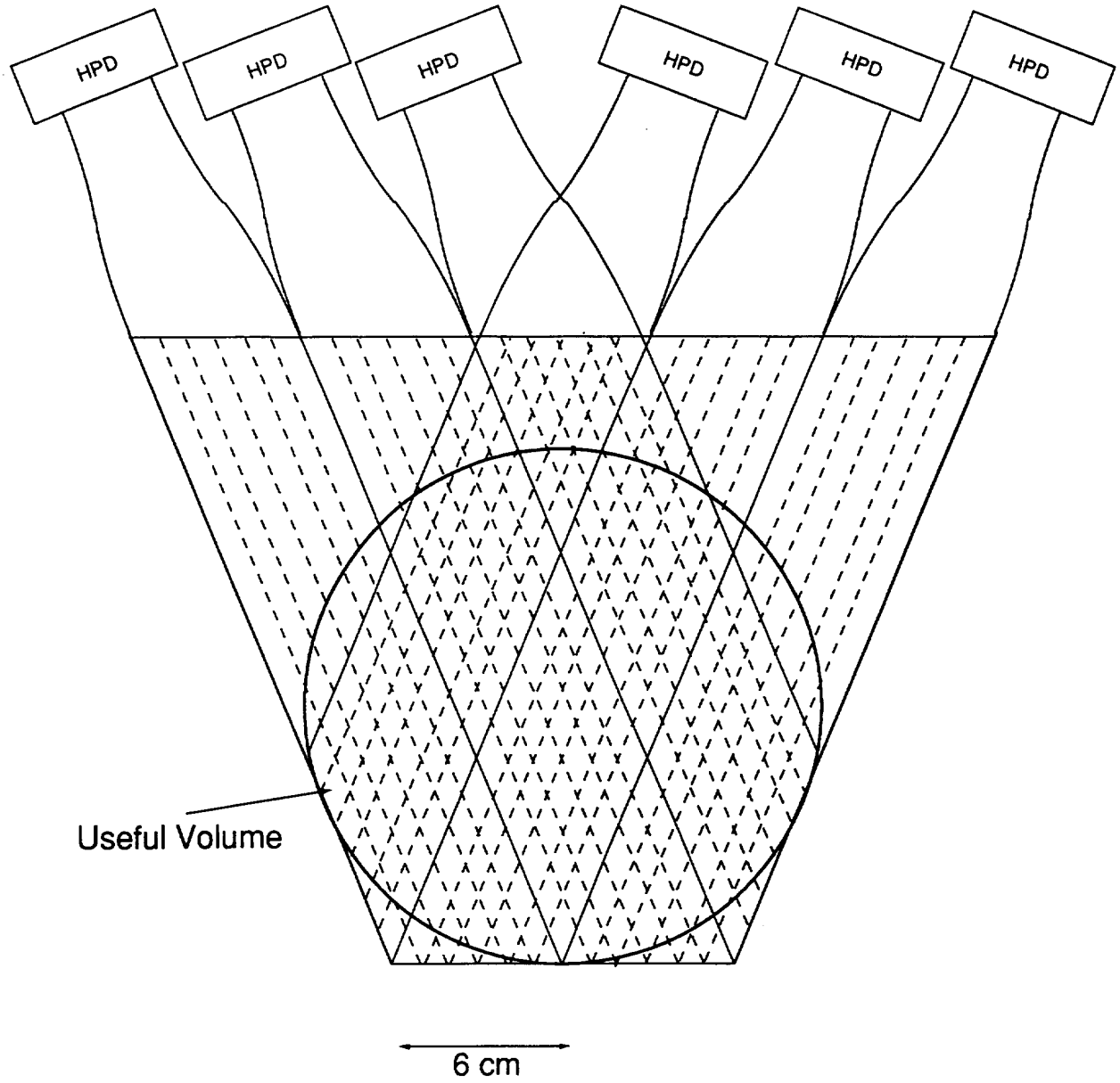

Figure 38